Optical transitions of symmetrical mixed-valence systems in the Class II–III transition regime†

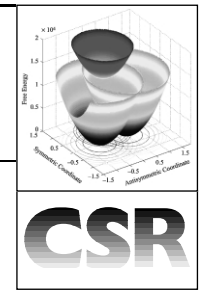

Bruce S. Brunschwig, Carol Creutz and Norman Sutin

Chemistry Department, Brookhaven National Laboratory, Upton, New York 11973-5000, USA

Received (in Cambridge, UK) 7th January 2002
First published as an Advance Article on the web 18th April 2002

In the Robin and Day classification, mixed-valence systems are characterized as Class I, II or III depending on the strength of the electronic interaction between the oxidized and reduced sites, ranging from essentially zero (Class I), to moderate (Class II), to very strong electronic coupling (Class III). The properties of Class I systems are essentially those of the separate sites. Class II systems possess new optical and electronic properties in addition to those of the separate sites. However, the interaction between the sites is sufficiently weak that Class II systems are valence trapped or charge localized and can the be described by a double-well potential. In Class III systems the interaction of the donor and acceptor sites is so great that two separate minima are no longer discernible and the energy surface features a single minimum. The electron is delocalized and the system has its own unique properties.

The Robin and Day classification has enjoyed considerable success and most of the redox systems studied to date are readily assigned to Class II. However the situation becomes much more complicated when the system shows borderline Class II/III behavior. Such "almost delocalized" mixed-valence systems are difficult to characterize. In this article spectral band shapes and intensities are calculated utilizing increasingly complex models including two to four states. Free-energy surfaces are constructed for harmonic diabatic surfaces and characterized as a function of increasing electronic coupling to simulate the Class II to III transition. The properties of the charge-transfer absorption bands predicted for borderline mixed-valence systems are compared with experimental data. The treatment is restricted to symmetrical ($\Delta G^0 = 0$) systems.

1 Introduction

In the late 1960s, the properties of molecular mixed-valence systems began to attract great interest because of the new

† Electronic supplementary information (ESI) is available: derivation of eqn. (39c), table summarizing the relationships between band maxima and band widths predicted by the two-state model and table of spectral properties of mixed-valence ruthenium(II)/(III) bridged by pyrazine and dicyanamide. See http://www.rsc.org/suppdata/cs/b0/b008034i/

Bruce Brunschwig was born in Philadelphia, Pa in 1944. He received his PhD from the Polytechnic Institute of Brooklyn in 1972. He joined the faculty of Hofstra University in 1972 . He took a leave of absence from Hofstra to work with Dr Norman Sutin at Brookhaven National Laboratory in 1977. In 1979 he joined the staff of Brookhaven where he is currently a Scientist in the Chemistry Department. His current research interests include studies of the kinetics and mechanism of thermal and photochemical charge-transfer reactions in solution.

Carol Creutz was born in Washington, D.C. in 1944. She studied chemistry at UCLA (BS 1966) and carried out her doctoral studies at Stanford (PhD 1971) with Henry Taube. She joined the Brookhaven National Laboratory Chemistry Department as a postdoctoral research associate in 1972, served as Department Chair 1995–2000, and is presently a Senior Chemist. Her research interests include mechanisms of reactions of transition metal complexes and their excited states, homogeneous catalysis in water; and charge transfer in nanoscale clusters.

Norman Sutin received his MSc degree from the University of Cape Town, South Africa, his PhD degree from Cambridge University, and held a postdoctoral research fellowship at Durham University, England. In 1956 Dr Sutin joined the Chemistry Department at Brookhaven National Laboratory as a Research Associate and retired as a Senior Chemist in September, 2001. His research interests include the kinetics and mechanisms of thermal and light induced electron transfer reactions of metal complexes.

Bruce Brunschwig

Carol Creutz

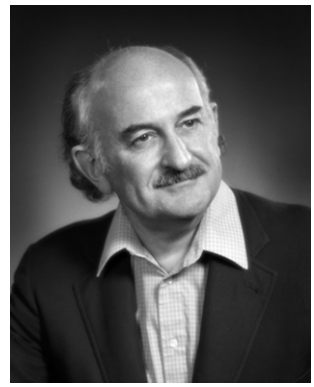

Norman Sutin

 DOI: 10.1039/b008034i

properties exhibited when significant electron coupling between the donor and acceptor sites is present and because of the relationships between the optical properties and electron transfer rates of the species.[1,2] Mixed-valence molecules contain donor (D) and acceptor (A) sites separated by a bridge (B).

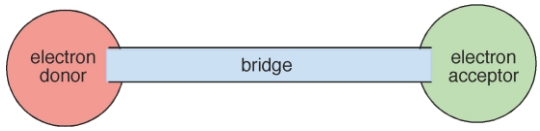

Most are based on d^6–d^5 metal centers, generally Ru(II)/Ru(III).[3–5] Systems of this type are therefore the focus of this article.

Since the 1990s the field has experienced a renaissance as a consequence of the synthesis and characterization of novel donor–acceptor systems, particularly those based on purely organic species and those at the borderline between Class II and III.[6–11] Indeed modeling/interpreting the behavior of systems in the Class II to III transition regime poses a formidable challenge.

The theory of electron transfer reactions has been presented in many texts and articles.[12,13] Here we consider the concepts relevant to the description of symmetric mixed-valence molecules and the energies and shapes of their donor–acceptor (metal-to-metal charge transfer, MMCT) absorption bands. We also consider the limitations of the traditional two-state model and the effects of introducing a third and fourth electronic state derived from electron transfer to or from a bridging group.

Several recent studies have focused on comparison of the shapes of the experimental intervalence bands in mixed-valence systems with the predictions of the two-state model. The systems studied include bishydrazine derivatives,[7] bistriarylamine derivatives,[6] and a variety of bridged organic and transition-metal systems.[8] It was noted that an improved fit of the asymmetric charge transfer spectra and intramolecular electron transfer rate constants for the bishydrazine radical cations could be obtained using quartic-augmented diabatic energy surfaces. Such a treatment yields absorption bands that are narrower on the low-energy side.[7] Band asymmetry ascribable to large electronic interaction was not considered. Despite the improved agreement obtained with the quartic term, the authors caution that there is no particular significance to this type of correction—other functions may fit as well.[14,15] Recently it has been shown that the band asymmetry is a natural result of combining harmonic diabatic states in the strong interaction region.[6,15]

In this article the classical model for MMCT band asymmetry is extended and spectral band shapes and intensities are calculated for increasingly complex models including two to four states. Free-energy surfaces are constructed utilizing harmonic diabatic (zero-order) states that satisfy the Generalized Mulliken–Hush condition that the transition moment connecting diabatic states be zero.[16] The surfaces are then characterized as a function of increasing electronic coupling to simulate the Class II to III transition. A Boltzmann distribution over the ground state surface is assumed and the properties of the charge-transfer absorption bands predicted for borderline mixed-valence systems are compared with experimental data. We first consider a two-state system consisting only of an initial and a final state or a ground and one excited state. For conciseness, we restrict the discussion to symmetrical (ΔG^0 = 0) systems; however, the treatment can readily be extended to unsymmetrical systems in which the electron transfer is accompanied by a net free energy change. We note that this treatment is based on a classical limit; starting from a quantum mechanical limit is another point of departure.[17]

Describing and classifying mixed-valence systems

Consider a mixed-valence molecule that has a symmetric bridge and two redox sites (the donor and acceptor sites) that are identical except for their oxidation states, for example, $(NH_3)_5Ru^{II}$-NC_5H_4-C_5H_4N-$Ru^{III}(NH_3)_5^{5+}$, where NC_5H_4-C_5H_4N is 4,4′-bipyridine. Due to this difference the equilibrium intramolecular and solvent configurations differ at the donor and acceptor sites. As a consequence the two sites are not equivalent and there exists a barrier to their interconversion. Because electron motion is much faster than nuclear motion, energy conservation requires that, prior to the actual electron transfer, the nuclear configurations of the reactants and the surrounding medium adjust from their equilibrium values to an intermediate configuration in which there is no energy change when the electron transfers from the donor to the acceptor. For metal complexes in a polar solvent, the nuclear configuration changes involve adjustments in the metal–ligand and intraligand bond lengths and angles, and changes in the orientations of the surrounding solvent molecules. Similar adjustments are also required in purely organic systems. In common with other chemical reactions, the intramolecular electron transfer reaction can be described in terms of the motion of the system on an energy surface from the initial to the final state *via* the activated complex (transition state). The electronic interaction of the sites will be very weak, and their interconversion slow, when the sites are far apart or their interaction is symmetry or spin forbidden.

The interconversion of the two states of a weakly coupled mixed-valence system is both an isomerization and a charge-transfer reaction.

$$DBA \rightleftharpoons D^+BA^- = ABD \qquad (1)$$

In either case the distortions of the initial and final states of the mixed-valence system can be described in terms of displacements on harmonic free-energy curves with identical force constants. This is illustrated in Fig. 1 where the free energy of

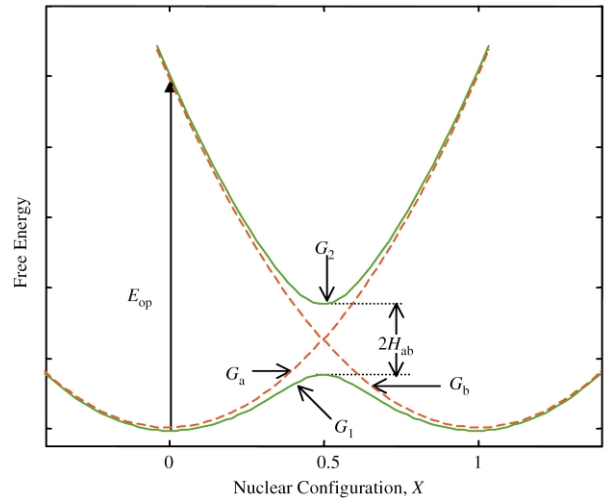

Fig. 1 Plots of the free-energies of the initial (left-hand parabola, G_a) and final (right-hand parabola, G_b) diabatic states and the lower (G_1) and upper (G_2) adiabatic states of a symmetric mixed-valence system *vs.* the reaction coordinate. E_{op} is the energy of the donor–acceptor (metal-to-metal MMCT or intervalence IVCT) charge-transfer transition and H_{ab} is the electronic coupling matrix element between the two diabatic states.

the initial state (DBA) plus surrounding medium (Curve G_a, wave function ψ_a) and the free energy of the final state (ABD) plus surrounding medium (Curve G_b, wave function ψ_b) of a symmetric mixed-valence system are plotted *vs.* the reaction coordinate X. The force constants of the parabolas are equal to 2λ, where λ is the vertical difference between the free energies of the DBA and ABD states at the equilibrium configuration of

DBA (or ABD). λ is generally referred to as the reorganization parameter and X varies from 0 to 1 as the reaction proceeds.

The free energies G_a and G_b are the energies of the zero-order or diabatic states of the system and are related to X by

$$G_a = \lambda X^2 \quad (1a)$$

$$G_b = \lambda(X - 1)^2 \quad (1b)$$

The interaction of the zero-order states gives rise to two linear combinations, the first-order or adiabatic states,

$$\psi_1 = c_a\psi_a + c_b\psi_b \quad (2a)$$

$$\psi_2 = c_a\psi_b - c_b\psi_a \quad (2b)$$

where ψ_1 is the wave function for the lower (ground) and ψ_2 is the wave function for the upper (excited) adiabatic state (energies G_1 and G_2, respectively), and the mixing coefficients are normalized, *i.e.*, $c_a^2 + c_b^2 = 1$. The overlap integral S_{ab} is neglected (or is zero by construction). The energies of the adiabatic states, obtained by solving the two-state secular determinant, are given by

$$G_1 = \frac{1}{2}\left\{(G_b + G_a) - \left[(G_b - G_a)^2 + 4H_{ab}^2\right]^{1/2}\right\} \quad (3a)$$

$$G_2 = \frac{1}{2}\left\{(G_b + G_a) + \left[(G_b - G_a)^2 + 4H_{ab}^2\right]^{1/2}\right\} \quad (3b)$$

Utilizing eqn. (3), the difference between the adiabatic energies is given by

$$(G_2 - G_1) = [(G_b - G_a)^2 + 4H_{ab}^2]^{1/2} \quad (4a)$$

$$= \{[\lambda(1 - 2X)]^2 + 4H_{ab}^2\}^{1/2} \quad (4b)$$

As H^{ab} increases, the adiabatic minima shift toward 0.5 and are given by[18]

$$\frac{1}{2}\left\{1 - \left[1 - 4(H_{ab}/\lambda)^2\right]^{1/2}\right\}, \frac{1}{2}\left\{1 + \left[1 - 4(H_{ab}/\lambda)^2\right]^{1/2}\right\} \quad (4c)$$

As shown in Fig. 1, the splitting at the intersection is $2H_{ab}$ and the barrier to electron transfer is lowered by H_{ab}. The free energy of activation for interconversion of the sites is then

$$\Delta G^* = \frac{(\lambda - 2H_{ab})^2}{4\lambda} \quad (5a)$$

with corresponding rate constant

$$k_{et} = A\exp\left[-\frac{(\lambda - 2H_{ab})^2}{4\lambda RT}\right] \quad (5b)$$

where the prefactor A is dependent on the electronic coupling. For weak coupling ('nonadiabatic' electron transfer), the prefactor is an electron-hopping frequency equal to $[2H_{ab}^2/h][\pi^3/\lambda RT]^{1/2}$ while, for strong coupling ('adiabatic' electron transfer), the prefactor is determined by a nuclear vibration frequency ν_n. In cases where the direct donor–acceptor interaction is very small, H_{ab} can be enhanced through the perturbative mixing of the ground state with higher electronic states. This mechanism for increasing the electronic coupling is termed 'superexchange'. At the adiabatic minimum the separation of the adiabatic curves is λ, while the diabatic curves are separated by $\lambda[1 - 4(H_{ab}/\lambda)^2]^{1/2}$.

Three classes of systems may be distinguished depending on the magnitude of the electronic coupling of the donor and acceptor sites. In Class I systems the coupling is very weak and the properties of Class I systems are essentially those of the separate sites (*i.e.*, the adiabatic energy curves are very close to the diabatic curves). Activated electron transfer either does not occur at all or occurs only very slowly (because of the very small value of H_{ab}) with $\Delta G^* = \lambda/4$. The intensity of the optical electron transfer band is very weak. Class II systems ($0 < H_{ab} < \lambda/2$) possess new optical and electronic properties in addition to those of the separate reactants. They remain valence trapped or charge localized: the electron transfer processes range from nonadiabatic ($H_{ab} < 10\ cm^{-1}$) to strongly adiabatic ($H_{ab} > 200\ cm^{-1}$) with ΔG^* given by eqn. (5a). Eqn. (5) holds as long as the ground state is described by a double-well potential, *i.e.*, as long as the system remains valence trapped. In Class III systems the interaction of the donor and acceptor sites has become so large that the ground state has only a single minimum at $X = 1/2$. This is the delocalized case which occurs when $H_{ab} \geq \lambda/2$. The latter condition follows readily from the zero barrier limit ($\Delta G^* = 0$) of eqn. (5a).

The Class II–III transition

The transition state for a Class II system is symmetric with a nuclear configuration that is the average of the donor and acceptor sites and with the electron rapidly oscillating between the two sites. Consequently the transition state for a Class II system has Class III character. Within activated complex theory the transition state is in equilibrium with the initial state. The equilibrium constant for the conversion of a Class II system to the Class III (transition state) system [eqn. (6)] is then determined by the free energy of activation for the electron transfer [eqn. (7)]

$$\text{Class II} \rightleftharpoons \text{Class III} \quad K_{II,III} \quad (6)$$

$$K_{II,III} = \exp(-\Delta G^*/RT) \quad (7)$$

where ΔG^* is given by eqn. (5a). The electron hopping rate in the transition state may be estimated[13] from $2H_{ab}/h$, the frequency of oscillation between two degenerate diabatic states. Thus for a given value of λ, the electron hopping rate in the transition state for a Class II system is less than the rate for a single minimum (larger H_{ab}) Class III system. In this respect the electron is not fully delocalized in the transition state for a Class II system. As H_{ab} increases, the transition state for a Class II system ultimately merges with the initial and final state minima to form the single minimum of the Class III system. When $\Delta G^* \approx RT$, comparable amounts of Class II and Class III systems will coexist and the system should exhibit properties characteristic of both.

Dynamic considerations lead to a similar conclusion. For the present purpose we distinguish two limiting contributions to λ: slow modes usually associated with solvent reorientation, λ_0, which have a characteristic time of ~1–10 ps, and all other faster modes, $\Sigma\ \lambda_i$, typically collective translations and bond vibrations, that are coupled to the charge transfer.

$$\lambda = \lambda_0 + \Sigma\ \lambda_i \quad (8)$$

An operational definition for the Class II–III transition—that solvent modes are averaged but inner-shell modes are not—has been proposed by Demadis *et al.*[3,10,11] With this assumption, a system will show both Class II and Class III properties if the rate constant for adiabatic intramolecular electron transfer [calculated from eqn. (9)]

$$k_{et} = \nu_n\exp(-\Delta G^*/RT) \quad (9)$$

is intermediate between the solvent reorientation frequency (10^{11}–$10^{12}\ s^{-1}$) and typical bond vibration frequencies (10^{13}–$10^{14}\ s^{-1}$). This translates to $k_{et} \sim 10^{12}$–$10^{13}\ s^{-1}$ which, for $\nu_n \sim 10^{13}\ s^{-1}$, implicates a free energy barrier of the order of RT which yields $1 \geqslant 2H_{ab}/\lambda \geqslant [1 - (4RT/\lambda)^{1/2}]$. For a λ value of 8000 cm^{-1} (1 eV), the free energy barrier will be $< RT$ when $2H_{ab}/\lambda \geq 0.7$. Consequently, for the present purpose, systems for which $0.7 < 2H_{ab}/\lambda < 1$ can be considered to be in the Class II–III transition regime. If the vibrational barrier is much smaller than the solvent barrier, then the rate constant for electron transfer in the transition regime will be determined by the solvent reorientation frequency. There is good experimental evidence for this type of behavior[19] in bridged cluster systems.[20]

In a semiclassical framework, the lower frequency solvent modes are treated classically while the higher frequency vibrational modes can tunnel through the reorganization barrier. If an increasing electronic coupling first eliminates the solvent barrier (evidently requiring $\lambda_0 < \Sigma \lambda_i$) then in the intermediate regime where $\lambda_0 < 2H_{ab} < \lambda_0 + \Sigma \lambda_i$, the solvent configurations of the donor and acceptor sites will be averaged and solvent reorientation will no longer contribute to the thermal or optical barrier to electron transfer but the two redox sites will still be structurally distinct. Although we are not aware of a rigorous theoretical justification for this interpretation there are experimental observations consistent with such hybrid behavior.[10,11] Finally, although a system is considered fully delocalized when $2H_{ab} > \lambda$, it could still exhibit IR absorption characteristic of both Class II and Class III if the stretching vibrations of the bridging ligand acquire intensity through the transient charge localization associated with the out-of-phase combination of the relatively slow breathing vibrations of the terminal metal complexes. In effect, transient charge localization, sufficient to create a dipole across the bridging ligand on a time scale somewhat longer than associated with its stretching vibrations, could be occurring within the single broad energy minimum of a borderline Class III system.[3]

2 A two-state model for the charge-transfer transition

The intervalence charge-transfer transitions in Class II and Class III systems have different characteristics. In this section we consider the energy, intensity, and shape of the absorption bands in Class II, Class III, and borderline systems.

2.1 The charge-transfer band maximum

Since the vertical difference between the *diabatic* energies at the equilibrium configuration (adiabatic minimum) is[18] $\lambda[1 - 4H_{ab}/\lambda$, it follows from eqn. (4a) that the vertical difference between the *adiabatic* energies at the equilibrium configuration is equal to λ. This result is independent of H_{ab} for $H_{ab} \leq \lambda/2$. In other words, *the vertical difference between the free energies of the two states of a symmetrical mixed-valence system remains equal to* λ at either equilibrium configuration regardless of the magnitude of the electronic coupling as long as the system remains valence trapped.[21] *Although the repulsion of the upper and lower curves increases with* H_{ab}, this is exactly cancelled by the two minima moving closer together.

When the electronic interaction of the donor and acceptor centers is significant, it is useful to express $h\nu_{max}$ for a Class II system in terms of λ', the reorganization energy corrected for charge delocalization (*i.e.*, the 'actual' reorganization energy):[18]

$$h\nu_{max} = \lambda = \lambda' + 4H_{ab}^2/\lambda \quad (10)$$

The actual reorganization energy is related to λ by

$$\lambda' = \lambda(1 - 4H_{ab}^2/\lambda^2) \quad (11)$$

where the $(1 - 4H_{ab}^2/\lambda^2)$ term is the square of the charge transferred in the optical transition. In terms of eqn. (10), there are two contributions to the transition energy. The first is the reorganization energy *which decreases with the degree of charge delocalization* and the second is a consequence of the stabilization of the ground state and the destabilization of the excited state through the electronic interaction: *this contribution increases with the degree of charge delocalization*. These two effects of delocalization exactly cancel and the transition energy for Class II species remains equal to λ regardless of the degree of localization.

The above equations have interesting, albeit disconcerting, implications for the solvent dependence of the transition energy: for a Class II system the absorption band maximum is predicted to show the *full* solvent dependence regardless of the value of H_{ab}. By contrast, the energy of the optical transition in a symmetrical Class III system is given by

$$h\nu_{max} = 2H_{ab} \quad (12)$$

and the transition energy increases with the strength of the electronic interaction. By the same token, within the two-state model, H_{ab} for symmetrical Class III complexes can be obtained directly from the energy of the optical transition. Note that the optical transition in a symmetrical Class III system, although intense, no longer involves charge transfer and is therefore not accompanied by a net dipole-moment change and should show no solvent dependence. Instead the optical absorption involves transitions between delocalized molecular orbitals of the system.

2.2 The transition moment

The transition moment μ_{12} and the dipole moments μ_a and μ_b of the initial and final diabatic states are related by

$$\mu_{12} = c_a c_b (\mu_b - \mu_a) \quad (13)$$

where c_a and c_b are the coefficients of the wave functions introduced earlier.[21] Since $c_a c_b = H_{ab}/\nu_{max}$ at the initial state minimum[21] it follows that

$$\frac{H_{ab}}{\nu_{max}} = \left| \frac{\mu_{12}}{\mu_b - \mu_a} \right| \quad (14a)$$

For a Class III system c_a and $c_b = 1/\sqrt{2}$ and $\nu_{max} = 2H_{ab}$. Consequently μ_{12} for a Class III system is equal to $(\mu_b - \mu_a)/2$. Defining $r_{ab} \equiv |(\mu_b - \mu_a)/e|$ yields eqn. (14b).

$$H_{ab} = \frac{\nu_{max}|\mu_{12}|}{e r_{ab}} \quad (14b)$$

The diabatic dipole-moment difference $(\mu_b - \mu_a)$ is related to the measured dipole-moment change $(\mu_2 - \mu_1)$ by eqn. (15).

$$\mu_b - \mu_a = [(\mu_2 - \mu_1)^2 + 4\mu_{12}^2]^{1/2} \quad (15a)$$

Eqn. (15a) can be rearranged and, with eqn. (14a), yields

$$(\mu_2 - \mu_1)^2 = (\mu_b - \mu_a)^2[1 - 4(H_{ab}/\nu_{max})^2] \quad (15b)$$

For a Class III system ($\nu_{max} = 2 H_{ab}$), $\mu_2 - \mu_1 = 0$ while for Class II,

$$(\mu_2 - \mu_1) = (\mu_b - \mu_a)[1 - 4(H_{ab}/\nu_{max})^2] \quad (15c)$$

For a Class III system eqn. (15a) also yields $\mu_{12} = (\mu_b - \mu_a)/2$ when $2H_{ab} > \lambda$.

The dependence of $\mu_{12}/(\mu_b - \mu_a)$ on H_{ab} is illustrated in Fig. 2. Note the μ_{12} for a symmetrical Class II system is directly proportional to H_{ab} while μ_{12} for a Class III system is independent of H_{ab}.

2.3 The shape and the intensity of the charge transfer band

It follows from time-dependent perturbation theory (Fermi's Golden Rule) that the shape of an absorption band is determined by the square of the overlap of the vibrational wave functions of the ground and excited states weighted by the Boltzmann population of the ground state level, with each vibrational line broadened by the solvent reorganization term (λ_0). Here we use a classical approximation in which the distribution of systems over the ground state configurations is assumed to be con-

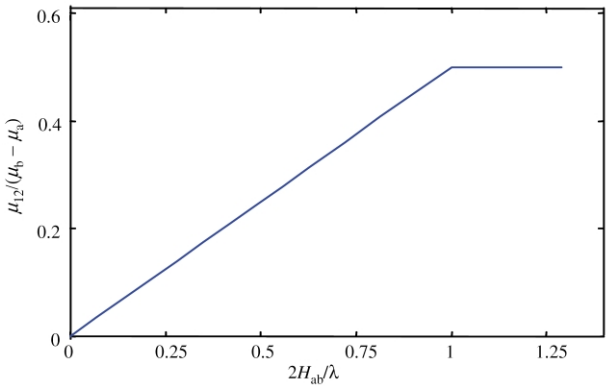

Fig. 2 Band intensity predictions of the two-state treatment.

tinuous. This approximation is valid when $h\nu_{in} \leq kT$. We first consider binuclear systems in which the electronic interaction of the donor and acceptor centers is negligible.

Weakly interacting centers. We assume that the interaction of the two centers is weak and that the energy of the system is adequately described by the zero-order parabolic surfaces. From a semiclassical viewpoint the molar absorptivity ε_{sc} (M^{-1} cm^{-1}) is given by[22]

$$\frac{\varepsilon_{sc}(\nu)}{\nu} = \frac{hBn(\nu)}{10^3 \ln(10) N c n_t} \tag{16}$$

where N is Avogadro's number, $n(\nu)/N$ is the molar concentration of species per unit frequency of the absorbed light possessing the nuclear configuration appropriate for the transition (*i.e.*, $n(\nu)d\nu$ is the molecular concentration of species able to absorb light in the frequency range ν to $\nu + d\nu$) and B, c and n_t are the Einstein coefficient of stimulated absorption, the speed of light, and the total molar concentration of absorbers, respectively. The Einstein coefficient and the transition dipole moment are related by

$$B = \frac{8\pi^3 |\mu_{12}|^2}{3h^2} \tag{17}$$

so that eqn. (16) and (17) yield

$$\frac{\varepsilon_{sc}(\nu)}{\nu} = \frac{8\pi^3 |\mu_{12}|^2 n(\nu)}{3\times 10^3 \ln(10) N h c n_t} \tag{18}$$

Assuming a Boltzmann distribution of systems over the ground-state energy surface gives

$$n(\nu) = n_0 \exp[-(\Delta G(\nu))/RT] \tag{19}$$

where $\Delta G(\nu)$ is the excess energy of a species on the ground-state surface as a function of the frequency of the absorbed light and $n_0 d\nu$ is the molecular concentration of absorbing species at the ground-state energy minimum. By use of eqn. (1a) we obtain

$$\Delta G(\nu) = G(\nu)_1 - G_{1,eq} = \lambda (X(\nu))^2 \tag{20}$$

where $G_{1,eq}$ is the value of G_1 at the ground-state equilibrium configuration. From eqn. (4b) the ground-excited-state energy difference $(G_2 - G_1)$ is related to X by

$$X(\nu) = \frac{\lambda - (G_2 - G_1)}{2\lambda} = \frac{\lambda - h\nu}{2\lambda} \tag{21}$$

Substitution into eqn. (19) gives

$$n(\nu) = n_0 \exp\left[-\frac{(\lambda - h\nu)^2}{4\lambda RT}\right] \tag{22}$$

These equations yield $n_0 = n_t hN / \sqrt{16\pi\lambda RT}$ where n_t, the total concentration of absorbers, is given by $n_t = \int_{-\infty}^{\infty} n(\nu) d\nu$. Substituting for $n(\nu)$ into eqn. (18) and assuming that the transition moment $\mu_{12} = \langle \Psi_2 | \mu | \Psi_1 \rangle$ does not depend on the vibrational level *i.e.*, on X, yields a Gaussian [eqn. (23)] for the band shape for ε/ν *vs.* ν in the weak interaction limit.

$$\frac{\varepsilon_{sc}(\nu)}{\nu} = \left(\frac{\varepsilon}{\nu}\right)_{max} \exp\left[-\frac{(\lambda - h\nu)^2}{4\lambda RT}\right] \tag{23a}$$

$$(\varepsilon/\nu)_{max} = 2\pi^3 |\mu_{12}|^2 / \left[3\times 10^3 \ln(10) c \sqrt{\pi\lambda RT}\right] \tag{23b}$$

In eqn. (23) $h\nu_0 = \lambda$ defines the maximum in the plot of $\varepsilon(\nu)/\nu$ *vs.* ν and corresponds to the energy of the vertical transition from the ground-state minimum. The half width (full width of the band at half height) of the band is given by

$$\Delta\nu^0_{1/2} = 2[4\ln(2)\lambda RT]^{1/2} \tag{24a}$$

At room temperature eqn. (24a) reduces to

$$\Delta\nu^0_{1/2} = [2310\lambda]^{1/2} \tag{24b}$$

In many treatments it is assumed that ν changes only slowly over the absorption band (*i.e.*, that the transition is very narrow compared to the energy of the transition, $\Delta\nu_{1/2} << \nu_{max}$) this yields $\varepsilon(\nu)/\nu \approx \varepsilon(\nu)/\nu_{max}$ which leads to

$$\varepsilon_c(\nu) = \varepsilon_{max} \exp[-(\lambda - h\nu)^2/4\lambda RT] \tag{25a}$$

$$\varepsilon_{max} = 2\pi^3 |\mu_{12}|^2 \nu_{max} / 3\times 10^3 \ln(10) c \sqrt{\pi\lambda RT} \tag{25b}$$

(We denote eqn. (25) as a classical treatment of the absorption while eqn. (23) is a semiclassical treatment.). Substitution for the constants and using eqn. (14b) gives the following expression for ε_{max} for a Gaussian–shaped band within the classical framework

$$\varepsilon_{max} = \frac{2.36\times 10^3 H_{ab}^2 r_{ab}^2}{\nu_{max} \Delta\nu^0_{1/2}} \tag{25c}$$

where ε_{max} is in $M^{-1}cm^{-1}$, H_{ab}, ν_{max}, and $\Delta\nu^0_{1/2}$ are in wave numbers and r_{ab}, the separation of the donor and acceptor charge centroids, is in Ångstroms. Rearranging eqn. (25c) yields the familiar Mulliken–Hush expression.

$$H_{ab} = 2.06\times 10^{-2} \frac{(\nu_{max} \varepsilon_{max} \Delta\nu^0_{1/2})^{1/2}}{r_{ab}} \tag{25d}$$

To the extent that $\Delta\nu_{1/2} << \nu_0$ the classical and semiclassical approaches yield the same results. In principle a plot of ε_{sc} vs $h\nu$ will not be Gaussian and its maximum will occur at higher energy than λ, so that the reorganization energy calculated from the halfwidth (evaluated from a plot of ε *vs.* $h\nu$) will not be correct; however, the errors will be small (a few per cent) for $\Delta\nu^0_{1/2} < 0.6\nu_{max}$. Thus, while the energy of the maximum in the plot of ε/ν *vs.* ν occurs at λ, when ε is plotted *vs.* ν the maximum ν_{max} occurs at $\lambda + 2RT$ for $\lambda > 8RT$. Similarly, $(\varepsilon/\nu)_{max}$, the maximum in the plot of ε/ν *vs.* ν, and ε_{max} are related by $\varepsilon_{max}/\nu_{max} = (\varepsilon/\nu)_{max}\exp(-RT/\lambda)$.

Strongly interacting centers. The situation is more complicated when the electronic coupling of the centers is appreciable. We again assume a Boltzmann distribution of systems over the ground-state energy surface but, as discussed earlier, the energy surfaces are no longer parabolic and the minimum of the initial state no longer occurs at $X = 0$. Moreover, as noted previously by Lambert and Nöll[6] and by Nelsen[8] the low-energy side of the absorption band is cut off at $h\nu = 2H_{ab}$, the minimum difference between the energies of the ground and excited states.

The relevant energy expressions for a symmetric mixed-valence system with appreciable electronic coupling are[18]

$$\frac{G_1}{\lambda} = \left(\frac{(1-2X)^2 + 1}{4}\right) - \frac{1}{2}\left[(1-2X)^2 + \left(\frac{2H_{ab}}{\lambda}\right)^2\right]^{1/2} \tag{26a}$$

$$\frac{G_2 - G_1}{\lambda} = \left[(1-2X)^2 + \left(\frac{2H_{ab}}{\lambda}\right)^2\right]^{1/2} \tag{26b}$$

and

$$\frac{G_{l,eq}}{\lambda} = -\frac{H_{ab}^2}{\lambda^2} \text{ for Class II} \quad (26c)$$

$$\frac{G_{l,eq}}{\lambda} = -\left(\frac{H_{ab}}{\lambda} - \frac{1}{4}\right) \text{ for Class III} \quad (26d)$$

Solving eqn. (26b) for $(1–2X)^2$ and substituting into eqn. (26a) yields:

$$G_l = \frac{1}{4\lambda}\left[\left((G_2 - G_1) - \lambda\right)^2 - 4H_{ab}^2\right] \quad (27a)$$

$$G_l - G_{l,eq} = \frac{1}{4\lambda}\left[(G_2 - G_1) - \lambda\right]^2 \text{ for Class II} \quad (27b)$$

and, for Class III,

$$G_l - G_{l,eq} = \frac{1}{4\lambda}\left[\left((G_2 - G_1) - \lambda\right)^2 - (2H_{ab} - \lambda)^2\right] \quad (27c)$$

Assuming a Boltzmann distribution over the energies on the *adiabatic* ground-state surface and using eqn. (19), (27b) and (27c) and integrating from $2H_{ab}$ to infinity yields:

$$n_0 = \frac{n_t N h}{\sqrt{4\pi\lambda RT}[1 - \text{erf}(z)]}\left\{\exp\left[\frac{(2H_{ab} - \lambda)^2}{4\lambda RT}\right]\right\} \quad (28)$$

where 'erf' is the error function, $z = (2H_{ab} - \lambda)/\sqrt{4\lambda RT}$, and the quantity in curly brackets is present only for Class III. Using eqns. (18), (27b) and (27c) yields the following expression for the shape of the band

$$\frac{\varepsilon(\nu)}{\nu} = \left(\frac{\varepsilon}{\nu}\right)_0 \exp\left[-\frac{(\lambda - h\nu)^2}{4\lambda RT}\right] \text{ for h}\nu \geq 2H_{ab} \quad (29a)$$

$$\frac{\varepsilon(\nu)}{\nu} = 0 \text{ for } h\nu < 2H_{ab} \quad (29b)$$

where

$$\left(\frac{\varepsilon}{\nu}\right)_0 = \frac{4\pi^3|\mu_{12}|^2}{3\times10^3 \ln(10)c\sqrt{\pi\lambda RT}[1 - \text{erf}(z)]} \quad (29c)$$

For Class II systems the error function can vary from ≈ -1 ($H_{ab} = 0$) to 0 ($2H_{ab} = \lambda$) while for Class III systems it varies from 0 ($2H_{ab} = \lambda$) to 1 ($2H_{ab} = \infty$). (Note that eqn. (29) is the correct form of eqn. (58d) in ref. 18. Figs. 11 and 12 in ref. 18 were constructed using the correct eqn. (29)). *Although the adiabatic energy surfaces for a strongly coupled system are far from parabolic, according to eqn. (29) the transitions are nevertheless described by a Gaussian-shaped band. The new feature introduced is the cut-off at* $2H_{ab}$. Note that, in a plot of ε/ν *vs.* ν, the experimentally observed molar absorptivity maximum for a Class II system occurs at $h\nu = \lambda$ and is given by

$$\left(\frac{\varepsilon}{\nu}\right)_{max} = \left(\frac{\varepsilon}{\nu}\right)_0 \quad (30a)$$

while the maximum for a Class III system occurs at $h\nu_{max} = 2H_{ab}$ and is given by

$$\left(\frac{\varepsilon}{\nu}\right)_{max} = \left(\frac{\varepsilon}{\nu}\right)_0 \exp\left[-\left(\frac{2H_{ab} - \lambda}{\sqrt{4\lambda RT}}\right)^2\right] \quad (30b)$$

Plots of $\varepsilon(\nu)/h\nu$ *vs.* $h\nu$ for a symmetric mixed-valence system are presented in Fig. 3.

The relative intensities of the intervalence band are also shown. As H_{ab} increases the band becomes truncated at low energy but, as long as $2H_{ab} < \lambda - [4\ln(2)\lambda RT]^{1/2}$ the width does not change, $\Delta\nu_{1/2} = \Delta\nu_{1/2}^0 = 2[4\ln(2)\lambda RT]^{1/2}$. Beyond this regime the observed full halfwidth $\Delta\nu_{1/2}$ decreases with increasing H_{ab}. For $2H_{ab} \leq \lambda$, the difference between the energies of the transition maximum and the energy corresponding to the half height of the band on the high energy side, $\Delta\nu_{hi}$, remains equal to $[4\ln(2)\lambda RT]^{1/2}$. Thus the full halfwidth of the band for a Class II system is given by

$$\Delta\nu_{1/2}^{II} = 2[4\ln(2)\lambda RT]^{1/2} = \Delta\nu_{1/2}^0 \quad (31a)$$

for $H_{ab} < 1/2(\lambda - \Delta\nu_{1/2}^0/2)$ and

$$\Delta\nu_{1/2}^{II} = [4\ln(2)\lambda RT]^{1/2} + (\lambda - 2H_{ab}) = \Delta\nu_{1/2}^0/2 + (\lambda - 2H_{ab}) \quad (31b)$$

for $H_{ab} > 1/2(\lambda - \Delta\nu_{1/2}^0/2)$. In the Class III region the width is given by

$$\Delta\nu_{1/2}^{III} = -(2H_{ab} - \lambda) + [(2H_{ab} - \lambda)^2 + 4\ln(2)\lambda RT]^{1/2} \quad (31c)$$

For $1 < 2H_{ab}/\lambda < (1 + \Delta\nu_{1/2}^0/4\lambda)$ (Class IIIA), eqn. (31c) reduces to eqn. (31b).The expressions for the band maxima and widths in the classical treatment are summarized in Table 1 where $\Delta\nu_{hi}$ and $\Delta\nu_{lo}$ refer to the energy difference between the band maximum and half-height points on the high and low frequency parts of the band. Unfortunately, in real systems the tails of intense (*e.g.* metal-to-ligand or ligand-to-metal charge transfer) bands at higher energy may make evaluation of $\Delta\nu_{hi}$ difficult. Unaware of the low-energy cut-off, experimentalists have sometimes evaluated $\Delta\nu_{lo}$ and doubled the value to obtain $\Delta\nu_{1/2}$. Additional relationships between the band maxima and halfwidths for the semiclassical treatment are given in supplementary Table 1.†

The Mulliken–Hush expression for H_{ab}, generalized to include strongly coupled systems, becomes

$$H_{ab} = 2.06\times10^{-2}\frac{\left(\nu_{max}\varepsilon_{max}\Delta\nu_{hi}(1 - \text{erf}(z)\right)^{1/2}}{r_{ab}} \quad (32a)$$

for Class II and

$$H_{ab} = 2.06\times10^{-2}\frac{\left(\nu_{max}\varepsilon_{max}\sqrt{4\ln(2)\lambda RT}(1 - \text{erf}(z)\right)^{1/2}}{r_{ab}} \quad (32b)$$

for Class III where z is defined above.

At $2H_{ab} = \lambda$, the Class II–III transition, the band retains intensity only in the high energy half of the unobserved 'full' Gaussian band, *i.e.*, the full width of the band at the Class II–III transition $(\Delta\nu_{1/2})^{II–III}$, is half of the full width of the Gaussian band in the Class I limit.

$$(\Delta\nu_{1/2})^{II–III} = [4\ln(2)\lambda RT]^{1/2} = \Delta\nu_{1/2}^0/2 \quad (33a)$$

Similarly, the expression for the electronic coupling element at the Class II–III transition, $(H_{ab})^{II–III}$, resembles eqn. (25d) but is for a 'half' Gaussian band

$$(H_{ab})^{II–III} = 2.06 \times 10^{-2}(\nu_{max}\varepsilon_{max}(\Delta\nu_{1/2})^{II–III})^{1/2}/r_{ab} \quad (33b)$$

Although the band is only half of a Gaussian, the electronic coupling element at the Class II–III transition is still given by the familiar Mulliken–Hush expression. Finally, the parameter Γ defined as

$$\Gamma = (1 - \theta) \quad (34a)$$

$$\theta = (\Delta\nu_{1/2})/(16\ln(2)\nu_{max}RT)^{1/2} = (\Delta\nu_{1/2})/(2310\nu_{max})^{1/2} \quad (34b)$$

where $\Delta\nu_{1/2}$ and ν_{max} are in wave numbers, provides a measure of the degree of delocalization. For Class II systems

$$\theta = (\Delta\nu_{1/2})/(\Delta\nu_{1/2}^0) \quad (34c)$$

and

$$\Delta\nu_{1/2} = \Delta\nu_{1/2}^0(1 - \Gamma) \quad (34d)$$

At low energies, when the cut-off does not decrease the bandwidth (*i.e.*, $2H_{ab} < \lambda - \sqrt{4\ln(2)\lambda RT}$), $\theta = 1$, $\Gamma = 0$. θ decreases to 0.5 and Γ increases to 0.5 at the Class II–III

transition. Consequently Γ is zero for a very weakly interacting system and 0.50 for a system at the Class II–III transition. For $2H_{ab}/\lambda$ between the cut-off value of $(1 - \Delta\nu^0_{1/2}/2\lambda)$ and unity (Class IIB) Γ is given by

$$\Gamma = 1/2 - (\lambda - 2H_{ab})/(\Delta\nu^0_{1/2}) \quad (34e)$$

The ratio θ introduced above is defined in the same spirit as **R** introduced by Nelsen.[8] However, in contrast to the earlier assignment,[8] the denominator of θ is not necessarily the high-temperature width of the absorption band. As is evident from the expression for the cut-off condition given above, the cut-off occurs *earlier* (*i.e.*, at smaller H_{ab}) at higher temperatures.

For $2H_{ab} > \lambda$, the Class III regime, only the high-energy side of the band remains and the highly asymmetric band shifts to higher energy and becomes increasingly narrow as H_{ab} increases. The observed maximum is now at $h\nu = 2H_{ab}$. Finally, when $2H_{ab} >> \lambda$ only a sharp line at $h\nu = 2H_{ab}$ remains and Γ approaches unity.

Calculated values of $\Delta\nu_{1/2}/\lambda$ and Γ are plotted *vs.* $2H_{ab}/\lambda$ for $\lambda/RT = 20$ and 40 in Fig. 4.

3 Comparison of the two-state model with experiment

We turn now to a comparison of predictions of the two-state models with experimental data for two families of diruthenium complexes, those bridged by a dicyanamide ($dicyd^{2-}$) and those bridged by a pyrazine (pz) ligand. As the metal–metal separation is essentially constant within a family (pz 6.9 Å; $dicyd^{2-}$ 13.2 Å), λ should also be essentially constant, but band narrowing is predicted as coupling increases. (Variations in the supporting ligands such as ammonia and pyridine introduce some variations in λ_i and λ_o.) The $dicyd^{2-}$-bridged complexes have recently been found to exhibit striking solvent sensitive

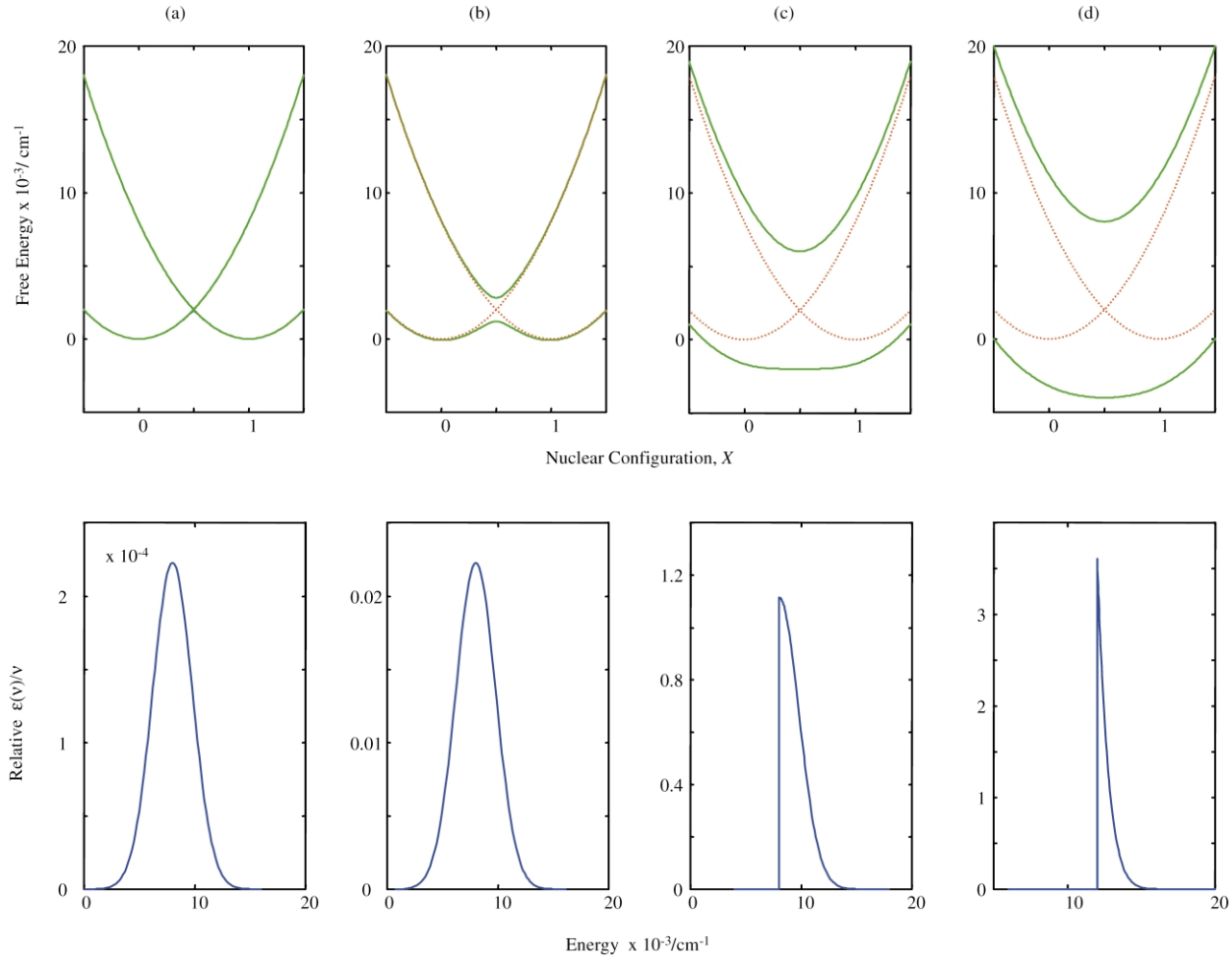

Fig. 3 Band shape predictions from the two-state treatment. Plots of free energy *vs.* the nuclear configuration coordinate X (top set) and relative $\varepsilon(\nu)/\nu$ *vs.* $h\nu$ (bottom set) for a symmetric mixed-valence system for increasing values of $2H_{ab}/\lambda$ with $\lambda = 8000$ cm^{-1}. The values of $2H_{ab}/\lambda$ (H_{ab}, cm^{-1} for (a), (b), (c) and (d) are 0.02 (80), 0.2 (800), 1.0 (4000) and 1.5 (6000), respectively. The values of $\varepsilon(\nu)/\nu$ are scaled to yield an oscillator strength proportional to the square of the calculated transition dipole moment, μ_{12}. The maximum values of $\varepsilon(\nu)/\nu$ for (a), (b), (c) and (d) are 2.2×10^{-4}, 2.2×10^{-2}, 1.1 and 3.6, respectively.

Table 1 Band maxima and widths[a] for different mixed-valence classes in a classical two-state treatment

Cut-off Location	Condition	ν_{max}	$\Delta\nu_{lo}$	$\Delta\nu_{hi}$
Class I	$2H_{ab}/\lambda << 1$	λ	$\Delta\nu^0_{1/2}/2$	$\Delta\nu^0_{1/2}/2$
Class IIA	$0 < 2H_{ab}/\lambda < (1 - \Delta\nu^0_{1/2}/2\lambda)$	λ	$\Delta\nu^0_{1/2}/2$	$\Delta\nu^0_{1/2}/2$
Class IIB	$(1 - \Delta\nu^0_{1/2}/2\lambda) < 2H_{ab}/\lambda < 1$	λ	$\lambda - 2H_{ab}$	$\Delta\nu^0_{1/2}/2$
Class II–III limit	$2H_{ab}/\lambda = 1$	$\lambda = 2H_{ab}$	0	$\Delta\nu^0_{1/2}/2$
Class IIIA	$1 < 2H_{ab}/\lambda < (1 + \Delta\nu^0_{1/2}/4\lambda)$	$2H_{ab}$	0	$\Delta\nu^0_{1/2}/2 + \lambda - 2H_{ab}$
Class III	$2H_{ab}/\lambda > 1$	$2H_{ab}$	0	Eqn. (31c)

[a] $\Delta\nu_{1/2} = \Delta\nu_{lo} + \Delta\nu_{hi}$; $\Delta\nu^0_{1/2}/2 = [4\ln(2)\lambda RT]^{1/2}$

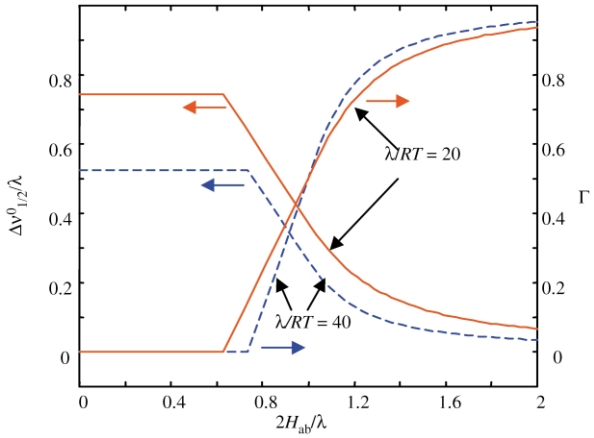

Fig. 4 Band width predictions from the two-state treatment. Plots of $\Delta\nu_{1/2}/\lambda$ (left axis) and Γ (right axis) *vs.* $2H_{ab}/\lambda$ for λ/RT = 20 and 40 (λ = 4000, 8000 cm^{-1}).

properties.[23] In the diruthenium(III) complexes, the oscillator strength of the LMCT transition and reduction potentials increase dramatically as solvent donor properties diminish and magnetic properties range from diamagnetic to paramagnetic. The mixed-valence complexes exhibit behavior ranging from Class II to borderline Class III to fully Class III, depending on substituents and solvent. Thus the pz- and dicyd^{2-}-bridged series provide an opportunity to study the Class II–III transition moderated by electron and hole superexchange mechanisms. For the pz-bridged complexes, MLCT and MMCT transitions are generally separated by $\geqslant$1 eV. By contrast for the dicyd^{2-} series, the LMCT band for the III, III complex and the MMCT band of the II, III complex are very similar in position. Thus, for purposes of describing the properties of the MMCT bands, a two-state model is expected to be more valid for the pz-series, while a three-state description might reasonably be expected to be necessary for the dicyd^{2-} series. However, to describe both MMCT and MLCT/LMCT band properties, a minimum of four states must be included. Three- and four-state treatments are presented later.

Intervalence band widths and maxima for mixed-valence Ru(II)/(III) complexes are summarized in supplementary Table 2.† ΔG^0_{com} values for Class(II)

$$Ru(II)–Ru(II) + Ru(III)–Ru(III) = 2Ru(II)–Ru(III) \quad (35a)$$

and for Class (III)

$$Ru(II)–Ru(II) + Ru(III)–Ru(III) = 2Ru(II.5)–Ru(II.5) \quad (35b)$$

(generally obtained from cyclic voltammetry) and literature assignments of the electronic ground state (Class II or III) are also included, along with Γ values calculated from the spectral data and the electronic structure previously assigned to the mixed-valence complex.†

The electronic structure (Class) assignments previously made for the mixed-valence complexes are in agreement with the 'prediction' obtained from Γ. The Γ values indicate that [{$Ru(NH_3)_5$}$_2$(μ-pz)]$^{5+}$ is a strongly coupled Class III system (Γ = 0.63) while the corresponding 4,4′-bpy-bridged complex is a weakly coupled Class II system (Γ = −0.1 in water). The pz-bridged species exhibit a wide range of behavior ranging from weakly coupled Class II (the ((phenX)$_2$RuCl)$_2$(μ-pz)$^{5+}$ series, Γ = −0.1 to −0.2, for example) to strongly coupled species at the Class II–III transition (the *trans*-($(NH_3)_4$LRu)$_2$(μ-pz)$^{5+}$ series, Γ = 0.5, for example). Similarly, the Me_2dicyd^{2-} and dicyd^{2-} bridged[9] [{*mer,mer*-$Ru(NH_3)_3$(bpy)}$_2$(μL)]$^{3+}$ complexes are assigned to Class III (Γ = 0.6) while the corresponding [{*trans,trans*-$Ru(NH_3)_4$(py)}$_2$(μ-L)]$^{3+}$ complexes are borderline Class II–III systems. Consistent with its Class III assignment the cyanamide stretching frequencies of [{*trans-,trans*-$Ru(NH_3)_4$(py)}$_2$(μ-Me_2dicyd)]$^{3+}$ in acetonitrile were recently shown to be the average of the corresponding frequencies of the fully oxidized and reduced complexes.[24] The dicyd^{2-} bridged complexes are generally strongly coupled Class II except for [{$Ru(NH_3)_5$}$_2$(μ-Cl_4dicyd^{2-})]$^{3+}$ which is weakly coupled (Γ = 0.4)(Table S2)†. Although similar Class assignments have been made on the basis of the comproportionation constants and the intervalence band intensities for the various systems, *the band shape criterion has the advantage of simplicity in that the concentration of the mixed-valence complex need not be known*. The band shapes and electronic coupling elements for the dicyd^{2-} derivatives have also been discussed by Nelsen with similar conclusions.[8]

Extent of delocalization

The transition from weakly coupled Class II to Class III is driven by increasing electronic interaction H_{ab}. As noted earlier, the value of Γ reflects whether a particular system is weakly coupled, moderately coupled Class II, at the Class II–III transition, or strongly coupled. For $\lambda \sim 8000$ cm^{-1} in a two-state model, these four regimes correspond to $0 < \Gamma < 0.1$, $0.1 < \Gamma < 0.5$, $\Gamma \approx 0.5$ and $\Gamma > 0.5$, respectively, at room temperature. For Class IIB and borderline Class II–III systems, $-\Delta G^0_{com} = 2H_{ab}^2/\lambda$.[25] From eqn. (34e), at room temperature $(-\Delta G^0_{com})^{1/2}$ and Γ are related by

$$(-\Delta G^0_{com})^{1/2}\ (cm^{-1/2}) = [(\lambda/2)^{1/2} - 17] + 34\Gamma \quad (35c)$$

As shown in Fig. 5 this relationship holds up fairly well for both dicyd^{2-}- and pyrazine-bridged diruthenium complexes in acetonitrile. (The comproportionation free-energy changes have been corrected for the statistical factor and for changes in the Coulomb repulsion of the metal centers using a point charge model.[25]) Slopes and intercepts for the dicyd^{2-} systems are 53, 24 $cm^{-1/2}$ in acetonitrile and nitromethane and 36, 28 $cm^{-1/2}$ in DMSO and acetone, respectively. For the pz system, the slope and intercept are 29, 34 $cm^{-1/2}$, respectively, for acetonitrile. Except for the dicyd^{2-} systems in acetonitrile and nitromethane, the slopes are close to the value predicted by eqn. (35c). The intercepts for the dicyd^{2-} systems yield $\lambda^{1/2}$ values of 58 and 64 $cm^{-1/2}$, somewhat smaller than the corresponding $(\nu_{max})^{1/2}$ values in Table S2.† By contrast, the intercept for the pz systems yields $\lambda^{1/2}$ of 78 $cm^{-1/2}$, in reasonable agreement with the $(\nu_{max})^{1/2}$ values.

Electronic coupling mechanisms

Within a superexchange framework the coupling in the pz and 4,4′-bpy-bridged complexes involves 'electron transfer' *via* the π*-LUMO of the bridging ligand while coupling in the dicyd^{2-} bridged complexes involve 'hole transfer' *via* the bridging ligand's π-HOMO. In the latter case replacing the coordinated ammonia by pyridine ligands increases the Ru(II)/(III) reduction potential thereby decreasing the energy gap for hole transfer and increasing the electronic coupling of the ruthenium centers. By contrast, replacing the electron donating $-CH_3$ by the electron-withdrawing Cl in the bridging ligand decreases the electronic coupling of the centers by making the bridge more difficult to oxidize.

In the strong coupling regime, there is little or no charge transfer associated with the 'intervalence charge-transfer transition'. Strongly coupled systems require a molecular orbital description, with intense transitions involving bonding (B), nonbonding (N), and antibonding (A) molecular orbitals. The character of the 'metal-to-metal charge-transfer transition' depends upon the metal–metal coupling mechanism. For the case of limiting MLCT superexchange, which involves vacant π* levels of the bridge, the MMCT transition becomes the bonding-to-nonbonding (B → N) transition. For the case of limiting LMCT superexchange, MMCT evolves to a nonbonding-to-antibonding (N → A) transition in the Class III

limit. The coupling schemes for pyrazine and $(CH_3)_2$dicyd^{2-} bridged diruthenium complexes[26,27] in Fig. 6 contrast MLCT and LMCT coupling mechanisms.

The electronic structures of strongly coupled systems can be related to those of analogous systems in the weakly coupled regime. For example, the band at 1570 nm in the spectrum of $(NH_3)_5RupzRu(NH_3)_5^{5+}$, for which Γ = 0.64, can also be described as the bonding-to-nonbonding (B $\rightarrow$ N) transition between molecular orbitals formed from the two Ru d_{xz} levels.[27] A much lower energy transition observed in the infrared region (ν_{max} = 2000 cm^{-1}, $\Delta\nu_{1/2}$ = 1400 cm^{-1}, ε = 300 M^{-1} cm^{-1}, Γ = 0.35)[28] may be described in terms of a localized nonbonding-to-nonbonding molecular orbital (n $\rightarrow$ N) transition. As another example, in the series of N_2-bridged diosmium complexes,[10] strong (π-backbonding) electronic interaction, along with spin orbit coupling, leads to a situation in which the bonding-to-antibonding transition of MMCT parentage is not directly observable because the antibonding levels are filled; however, the energies of these transitions, $2H_{ab}$ ~ 6500 cm^{-1}, can be estimated from the energies of observable transitions to the nonbonding d orbital hole.

High symmetry pentakis bridged mixed-valence complexes, such as the decaammine series, are particularly useful because their spectroscopy is simpler than that of the lower symmetry species. Recent work with pentacyano complexes has made possible comparison of the homologous series $[M(CN)_5]_2pz^{5-}$, M = Fe, Ru, Os.[29] The cyanide ligands confer extraordinarily solvent dependent thermodynamics on their complexes. While MMCT is difficult to observe for aqueous solutions, fairly stable mixed-valence complexes can be generated in organic solvents and their MMCT bands observed. Spectral assignments for $[Os(CN)_5]_2pz^{5-}$ in acetonitrile were made by analogy with assignments for $[(NH_3)_5M]_2pz^{5+}$ (M = Ru, Os). Thus the 7170 cm^{-1} band ($\Delta\nu_{1/2}$ = 1450 cm^{-1}) with Γ = 0.64 indicates a delocalized diosmium species. However vibrational data indicate valence trapping, at least on the vibrational timescale. The 4000 cm^{-1} band ($\Delta\nu_{1/2}$ = 1500 cm^{-1}, Γ = 0.51) was assigned to MMCT for $[Fe(CN)_5]_2pz^{5-}$ in acetonitrile. Vibrational spectroscopic studies again indicated borderline Class II–III behavior. By contrast, the 5682 cm^{-1} band assigned to MMCT for $[Ru(CN)_5]_2pz^{5-}$ in dichloromethane is broad ($\Delta\nu_{1/2}$ = 4200 cm^{-1}, Γ = −0.16), clearly indicating a Class II system. The three species have surprisingly similar values for electrochemically determined ΔG^0_{com}: 2742 (Os), 2582 (Fe), and 2260 (Ru) cm^{-1}. The cyclic voltammetry was conducted for millimolar solutions of complex in 0.1 M tetrabutylammonium hexafluorophosphate; for Os in acetonitrile at 298 K, for Fe in acetonitrile at 248 K, and for Ru in dichloromethane at 298 K. By contrast, the spectroelectrochemical measurements were made on *ca.* 0.5 M solutions of complex in acetonitrile at 298 K. If ion pairing is absent, the electrostatic correction to ΔG^0_{com} is much greater for the Ru complex in dichloromethane (1920 cm^{-1} *vs.* 240 cm^{-1} for acetonitrile at 298 K). It is not clear whether ΔG^0_{com} for Fe at 298 K would be greater or smaller than the value determined at 248 K. Thus, while it is not feasible to use the ΔG^0_{com} values in a quantitative way, it is clear that exploitation of the organic solvents of weak acceptor character makes it possible to observe significant metal–ligand and

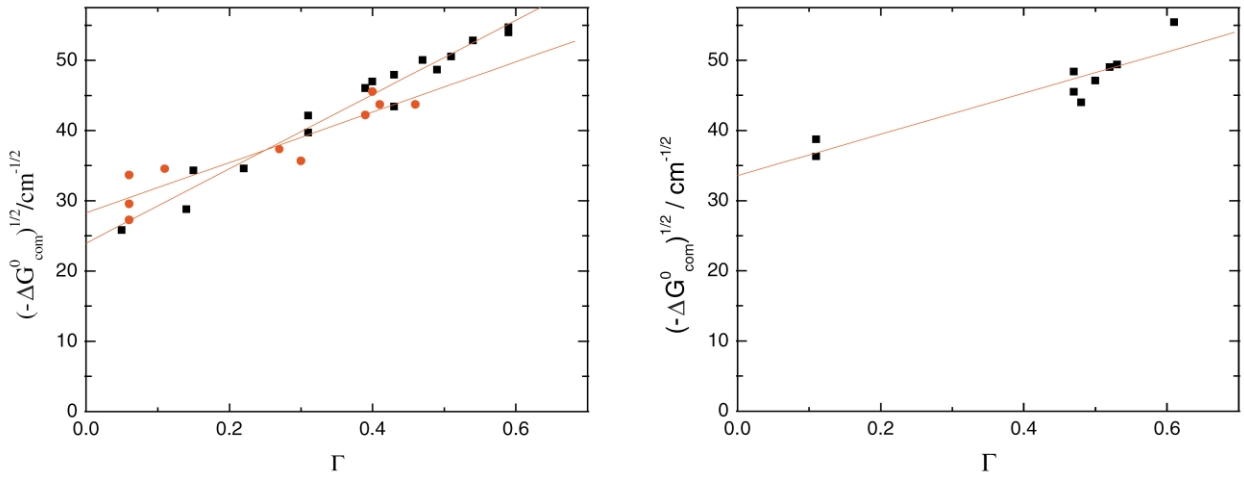

Fig. 5 $(\Delta G^0_{com})^{1/2}$ *vs.* Γ for dicyd^{2-}-bridged complexes (left) in CH_3CN and nitromethane (squares) and in dimethyl sulfoxide and acetone (circles) and (right) for pz-bridged mixed-valence complexes in CH_3CN.

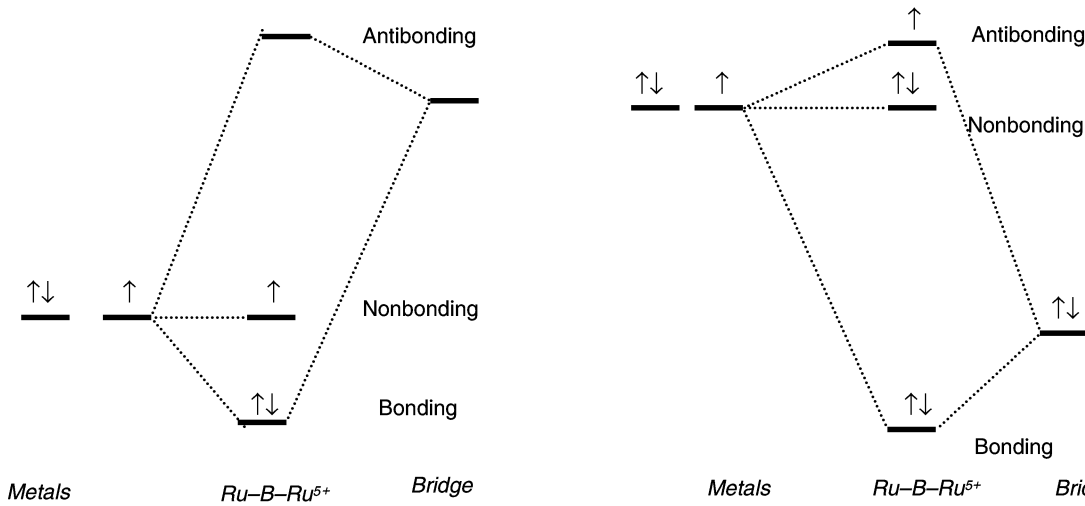

Fig. 6 Schematic molecular orbital diagrams for bridged mixed-valence complexes in which coupling involves the bridging ligand LUMO (MLCT, pz, left) and the bridging ligand HOMO (LMCT, dicyd^{2-}, right).

metal–metal coupling for the pentacyano series. These and related[30] studies also highlight the role of the ancillary (cyanide) ligands in modulating the M–pz backbonding interaction which decreases in the order Fe > Os > Ru for $M(CN)_5^{3-}$.

Comparison with spectroscopic parameters

Fig. 7 summarizes results of the two-state treatment directly applicable to the experimental data; normalized halfwidths,

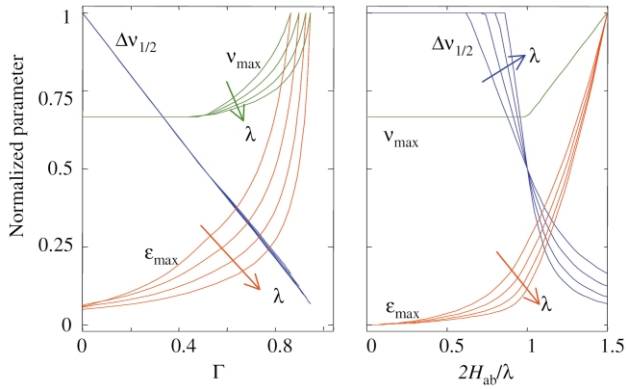

Fig. 7 Plots of normalized $\Delta\nu_{1/2}$, ν_{max}, and ε_{max} *vs.* Γ (left) and $2H_{ab}/\lambda$ (right) for λ = 4000, 8000, 16000, and 30000 cm^{-1}. The values of λ increase in the direction of the arrows. The quantities have been normalized by their largest value for a particular λ. The normalization values are $\Delta\nu^0_{1/2}$ for $\Delta\nu_{1/2}$ and ν_{max} and ε_{max} at $2H_{ab}/\lambda$ = 1.5 (its maximum value) for ν_{max} and ε_{max}, respectively. In the left hand plot, the values of the normalized $\Delta\nu_{1/2}$ for different λ values are very similar while the values of the normalized ν_{max} for different λ are the same in the right hand plot.

band maxima, and molar absorptivities calculated from the two-state model are plotted against Γ and $2H_{ab}/\lambda$. The halfwidth is thus predicted to be a linear function of Γ, even in the Class III regime, the slope and intercept of $-\nu^0_{1/2}$ and $+\nu^0_{1/2}$, respectively. ν_{max} is a constant (λ) in the Class II region and increases in Class III, $\Gamma > 0.5$. The value of ε_{max} is predicted to increase with H_{ab}^2 in Class II, and increases even more rapidly for Class III.

Band maxima

Experimental band maxima are presented in Fig. 8. For some of the very weakly coupled species, $\Gamma < 0$, indicating that the band is too wide in the weak coupling regime; spin-orbit splitting has been considered as a source of this broadening.[31] The dicyd^{2-} data do show a remarkable constancy of ν_{max}, even amongst the different series derived by successively replacing NH_3 by pyridyl ligands. By contrast, for the pz-bridged complexes, ν_{max} remains constant within a structure class, but is smaller for the tetraammine and pentaammine species. The Class III value of ν_{max} is predicted to increase with H_{ab} (H_{eff}) [eqn. (1)], a trend not especially evident in either data set. The λ values implicated for the different series do not reflect the behavior expected from a dielectric continuum model. Thus λ should decrease as coordination shell radius increases, *i.e.*, pentaammine > tetraammine > triammine; nearly the opposite behavior is found. λ_0 is predicted to increase as the solvent function $(1/D_{op}–1/D_s)$. Such dependencies have been reported,[4,5] but for the tabulated dicyd^{2-} data, which are of a magnitude consistent with the dielectric continuum model, this dependence is not detectable. Breakdown of simple dielectric continuum solvent behavior[32] is expected when the donor/acceptor radii are greater than the donor/acceptor separation. Ion pairing can confound studies in low-dielectric organic solvents. Specific solvent effects evidently dominate many systems.[33]

Band shapes

To summarize the principal features of the intervalence band shape for symmetrical systems predicted by the classical two-state model: For a very weakly interacting system, the band is Gaussian shaped with $\Gamma \sim$ zero and full-width-at-half-height, $\Delta\nu^0_{1/2}$. As H_{ab} increases, the band becomes truncated on the low-energy side, but Γ remains equal to zero until the cut-off starts to decrease the full width at half height. As H_{ab} increases further, Γ approaches 0.50, the value for a system at the Class II–III transition, and $\Delta\nu_{1/2} \sim 0.5\ \Delta\nu^0_{1/2}$.

Data for dicyd^{2-} (left) and pz (right) are plotted in Fig. 9. From eqn. (31), the plots of $\Delta\nu_{1/2}$ *vs.* Γ for Class II and Class II–III systems with constant ν_{max} should be linear with intercept = −(slope) = $\Delta\nu^0_{1/2} = (2310\lambda)^{1/2}$. For dicyd, slope = $-(3.8 \pm 0.1) \times 10^3$ cm^{-1} and intercept = $(3.96 \pm 0.04) \times 10^3$ cm^{-1}, consistent with $\lambda = 6.6 \times 10^3$ cm^{-1}. For pz, slope = $-(4.4 \pm 0.4) \times 10^3$ cm^{-1} and intercept = $(4.1 \pm 0.2) \times 10^3$ cm^{-1}, consistent with $\lambda = 7.9 \times 10^3$ cm^{-1}.

Band intensity

For the two-state treatment in the weak coupling limit, ε_{max} and f_{os} ($= 4.6 \times 10^{-9}\ \varepsilon_{max}\Delta\nu_{1/2}$, for a Gaussian; $\varepsilon(M^{-1}cm^{-1}$, $\Delta\nu_{1/2}$, cm^{-1}) are predicted to increase as H_{ab}^2 [eqn. (25c)]. Near the Class II–III transition, they are proportional to H_{ab}. In the Class III regime, μ_{12} is constant ($= (\mu_a - \mu_b)/2$) (Fig. 2), while ε_{max} continues to increase with H_{ab}. Since the band narrows with increasing H_{ab}, ε_{max} should increase with increasing $H_{ab} = E_{op}$ (Fig. 3). However, since no significant variation in E_{op} is found (Fig. 8) for either L series at $\Gamma \sim 0.5$, ε_{max} should be

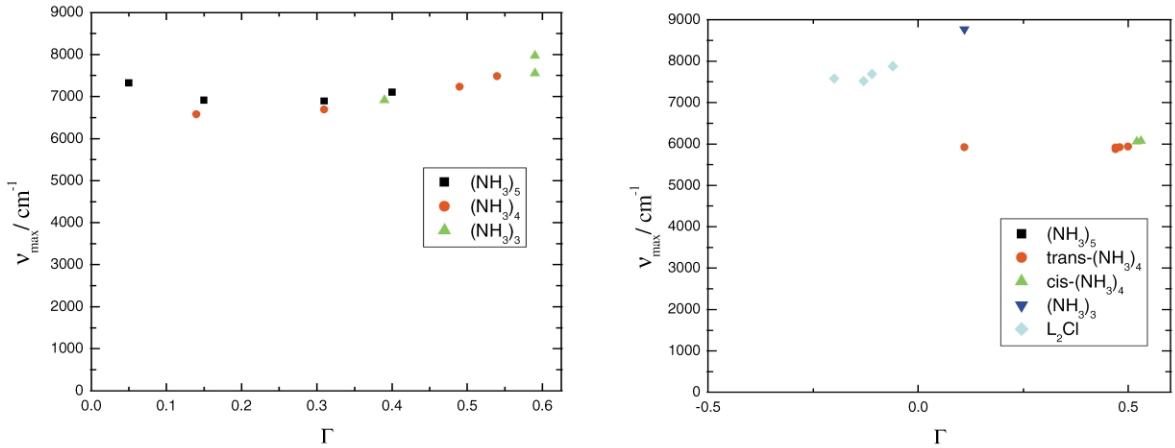

Fig. 8 ν_{max} as a function of Γ for dicyd^{2-}-bridged (left) and pz-bridged mixed-valence complexes (right) in acetonitrile.

essentially constant if the $\Gamma = 0.5$ species are Class III. The expected increase in ε_{max} with Γ for Γ between 0 and 0.5 is observed for both bridges, as illustrated in Fig. 10. For the dicyd^{2-}-bridged species ε_{max} seems to level off and decrease at high Γ, but no such trends are evident for the pz-bridged complexes. The band oscillator strengths are much smaller, however, for the pz-bridged complexes (upper value *ca.* 0.1) compared to the dicyd^{2-}-bridged species (upper value *ca.* 0.3), consistent with the smaller value of the diabatic transition moment for pz (short length).

In summary, the trends in Figs. 8–10 indicate that the two-state analysis of the shapes of the MMCT bands of the two series of bridged, binuclear ruthenium mixed-valence complexes is a useful and apparently valid one. A two-state treatment does not, however, address other absorption features of the complexes or the mechanism for the (bridge-mediated) electronic coupling of the metal sites. To address these interesting and important issues, additional states must be considered.

4 A three-state model for the charge transfer transition

We next consider the formalism for bridged mixed-valence systems in which the electron transfer is mediated by a third state formed by charge transfer to or from the bridging group. When the mediating state is of high energy the electron transfer can be treated analytically by invoking perturbative (super-exchange) mixing of the reactant, product and mediating states: the wave functions for the former diabatic states are modified by including perturbative contributions from the higher electronic states. On the other hand, if the mediating state is sufficiently low lying, charge transfer can take place by a sequential electron or hole transfer reaction (chemical mechanism) in which the bridging group becomes reduced [eqn. (36a)] or oxidized [eqn. (36b)], see Fig. 6.

$$DBA \rightarrow D^+B^-A \rightarrow D^+BA^- \quad (36a)$$

$$DBA \rightarrow DB^+A^- \rightarrow D^+BA^- \quad (36b)$$

In general, a 3×3 Hamiltonian must be solved. For a three-state system in which the third state lies at intermediate energy a numerical approach is used here.

Free-energy surfaces

As discussed above, the impact of the third state depends upon its energy relative to the other two diabatic states: ΔG^0_{ac} is the minimum (a or b)-to-minimum (c) energy difference. Because of the symmetry of the situation considered here, the third state minimum lies directly above the intersection of the diabatic curves at $X = 1/2$; it may however lie outside the x–y plane. Here, the third state is assumed to have the same force constant as the other two diabatic states (which are the same as those considered for the two-state model).

We first consider two cases depending on whether the mediating state lies above or just below the intersection of the reactant and product diabatic states. These situations are illustrated in Figs. 11 and 12, respectively, in which only

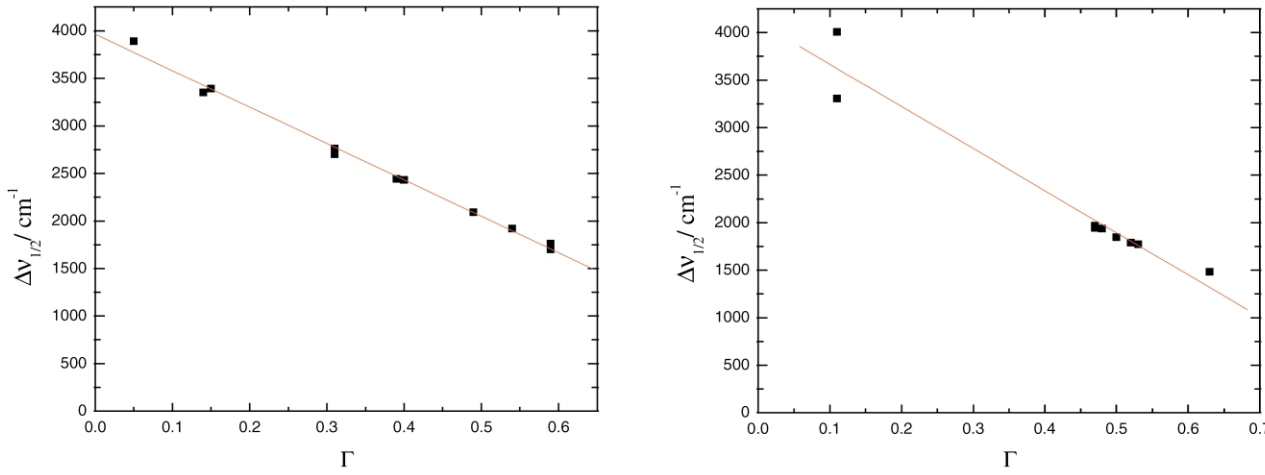

Fig. 9 Plots of $\Delta\nu_{1/2}$ *vs.* Γ for dicyd^{2-}-bridged (left) and pz-bridged mixed-valence complexes (right) in acetonitrile.

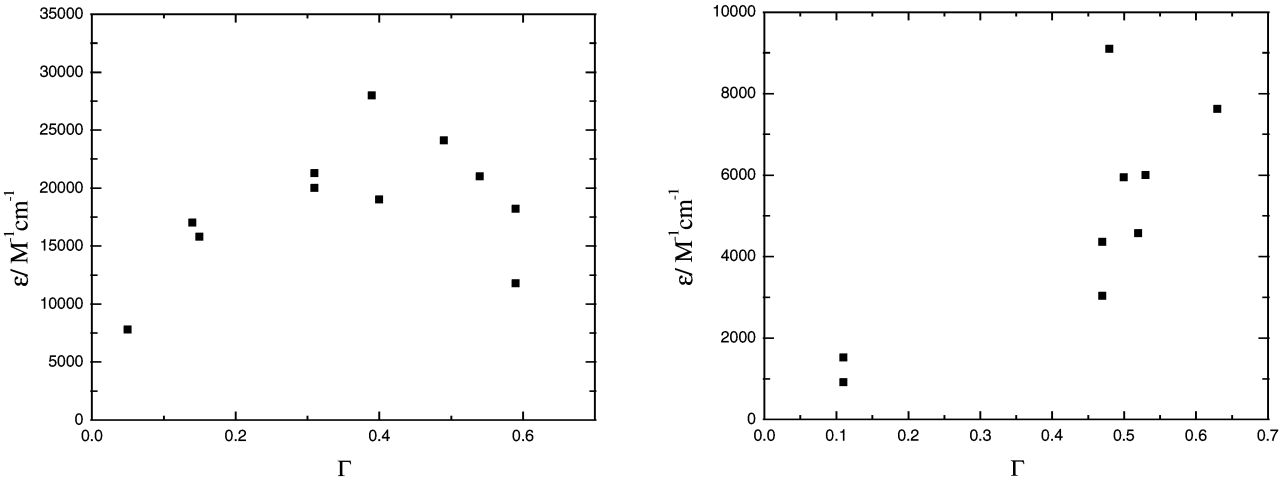

Fig. 10 Plots of ε *vs.* Γ for dicyd^{2-}-bridged (left) and pz-bridged mixed-valence complexes (right) in acetonitrile.

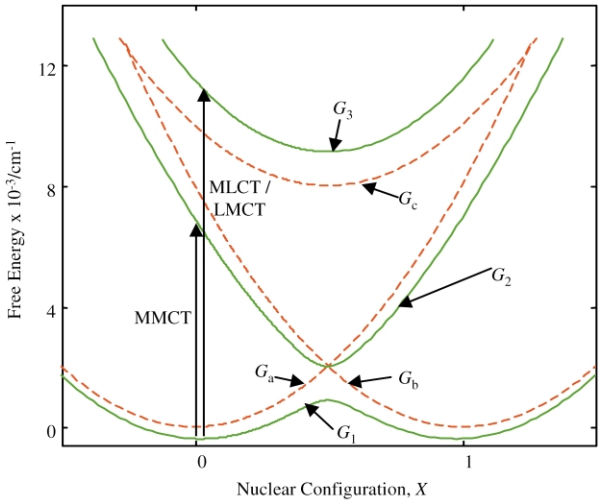

Fig. 11 Diabatic (dashed lines) and adiabatic (solid lines) free-energy curves for a three-state system with ΔG^0_{ac} = 8000 cm^{-1}, H_{ac} = H_{bc} = 2000 cm^{-1} (λ = 8000 cm^{-1}). The energies of the MMCT and MLCT transitions are also shown.

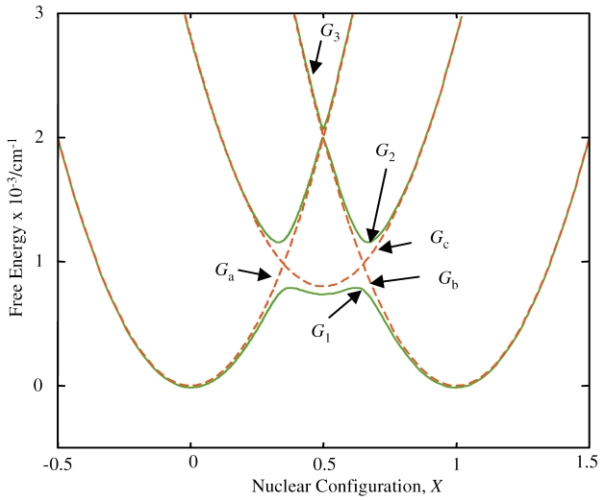

Fig. 12 Diabatic (dashed lines) and adiabatic (solid lines) free-energy curves for a three-state system with ΔG^0_{ac} = 800 cm^{-1}, H_{ac} = H_{bc} = 200 cm^{-1} (λ_{ab} = 8000 cm^{-1}, λ_{ac} = 2000 cm^{-1}).

coupling between the bridge (c) and the reactant and product (a,b) diabatic states is considered, *i.e.*, H_{ab} = 0. The dashed lines are the diabatic states while the solid lines are the adiabatic states obtained from calculations of a three-state model with the parameters given in the figure caption. At the nuclear configuration corresponding to the intersection of the reactant and product diabatic states the energy of the middle adiabatic state is in each case equal to that of the intersection, *i.e.*, it is 'noninteracting' at the nuclear configuration of the intersection. Contrary to the case for direct coupling of two diabatic states (Fig. 1), the separation of the lower and middle adiabatic states at the intersection of the reactant and product diabatic states (H_{ac} = H_{bc}) is not symmetric about the intersection: the lowest adiabatic state is stabilized while the energy of the middle state does not change. As the coupling (H_{ac} and H_{bc}) increases, the minima of the lowest three-state surface approach one another as was earlier seen for the two-state model.

It is evident from Fig. 12 that when the mediating state is sufficiently low lying, the middle adiabatic state develops a double minimum and the low energy adiabatic state develops a third minimum between the reactant and product states. In this case the mediating state may be of sufficient stability to be populated as an intermediate in the overall electron transfer reaction (chemical mechanism) as discussed above.

In the intersection region the three-state problem can be solved *analytically*. When the reactant–bridge and product–bridge couplings are equal (H_{ac} = H_{bc}) and the reactant–product coupling, H_{ab}, is zero, the separation between the adiabatic surfaces at X = 1/2 is given by

$$(G_2 - G_1)_{X=0.5} = -\frac{\Delta G_g}{2} + \frac{\left(\Delta G_g{}^2 + 8H_{ac}^2\right)^{1/2}}{2} \qquad (37a)$$

$$(G_3 - G_1)_{X=0.5} = (\Delta G_g{}^2 + 8H_{ac}^2)^{1/2} \qquad (37b)$$

where ΔG_g is the difference between the energy of the diabatic high-energy state and the energy of the reactant and product diabatic states at the intersection, *i.e.*, $\Delta G_g = G_c - G_b = G_c - G_a$. If $\Delta G_g >> H_{ac}$, H_{bc} we obtain

$$(G_2 - G_1)_{X=0.5} = \frac{2H_{ac}^2}{\Delta G_g} = \frac{2H_{bc}^2}{\Delta G_g} = \frac{2H_{ac}H_{bc}}{\Delta G_g} \qquad (38)$$

When ΔG_{ac} and ΔG_{bc} >> H_{ac} = H_{bc} and H_{ab} = 0, the three-state description approaches an 'equivalent' two-state (superexchange) treatment with the effective coupling between the two states, H_{eff}, given by[34,35]

$$H_{eff} = \left(\frac{H_{ac}H_{bc}}{\Delta G_{eff}}\right)_X \qquad (39a)$$

$$\left(\frac{1}{\Delta G_{eff}}\right)_X = \frac{1}{2}\left(\frac{1}{\Delta G_{ac}} + \frac{1}{\Delta G_{bc}}\right) \qquad (39b)$$

The effective coupling in the superexchange treatment is a function of the nuclear configuration of the system through the dependence of ΔG_{eff} on X. The 'equivalent' two-state approximation breaks down as H_{eff} increases due to either increasing H_{bc} or H_{ac} or decreasing ΔG_{eff}.

The three-state and 'equivalent' two-state surfaces are compared in Fig. 13. When H_{eff} is small (*i.e.*, the energy of the

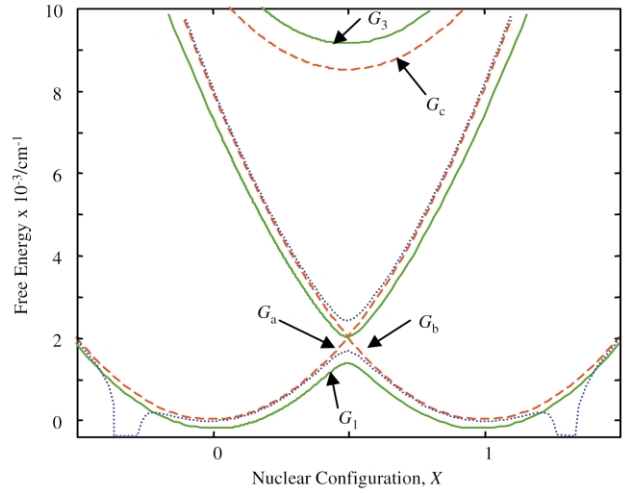

Fig. 13 Diabatic (dashed lines) and adiabatic (solid lines) free-energy curves for a three-state system with ΔG^0_{ac} = 8500 cm^{-1}, H_{ac} = H_{bc} = 1500 cm^{-1} (λ_{ab} = 8000 cm^{-1}, λ_{ac} = 2000 cm^{-1}). The equivalent two-state energy curves are shown as dotted lines.

mediating state is high compared to the coupling), the 'equivalent' two-state surface parallels the low energy three-state surface, but is displaced to higher energy for X between 0 and 1. The separations of the two lower adiabatic surfaces are the same at X = 1/2 in the 'equivalent' two-state and three-state treatments. However, for small or large values of X the energy of the reactant or product state can approach that of the bridging state [eqn. (39)], ΔG_{eff} = 0) and produce singularities in the 'equivalent' two-state surface (protuberances in Fig. 13).

Absorption band energies, shapes, and intensities

To calculate the absorption profiles we assume a Boltzmann distribution of systems on the ground-state surface (as before). The resulting free-energy surfaces and absorption profiles are compared in Fig. 14. Note that the mediating third state can be either metal-to-ligand charge transfer [MLCT, eqn. (36a)] or ligand-to-metal charge transfer (LMCT, eqn. (36b)) in nature. It is evident from Fig. 14 that both the MMCT and the MLCT/LMCT transitions increase in intensity with increasing H_{ac} in the Class II regime. At the Class II–III transition, the MLCT/LMCT intensity has vanished and the 'MMCT' transition has become narrow and intense. The shifts in E_{op} and band width with increased coupling in the three-state treatment are shown in Fig. 15. (While the perturbative formalism suggests that E_{op} and $\Delta\nu_{1/2}$ should be plotted against $H_{ac}^2/(\Delta G_{eff}\,\lambda)$, plots such as those in Fig. 15 show a more systematic behavior when $H_{ac}^2/(\Delta G_{ac}^0\lambda)$ is used.)

It is evident from Fig. 15 that, for systems similar to these illustrated in Fig. 11, the MMCT band maximum decreases in energy as H_{ac} ($= H_{bc}$) increases in the Class II region. This occurs because increased coupling decreases the energy of the two metal-centered states G_1, G_2 and increases the energy of the mediating state G_3. The effect is larger for the product state than it is for the reactant state since the energy gap between the mediating state and the product state is smaller. Thus the energy difference, E_{op}, ($= G_2 - G_1$) between the reactant and product state decreases. Note that increasing H_{ac} ($= H_{bc}$) and decreasing

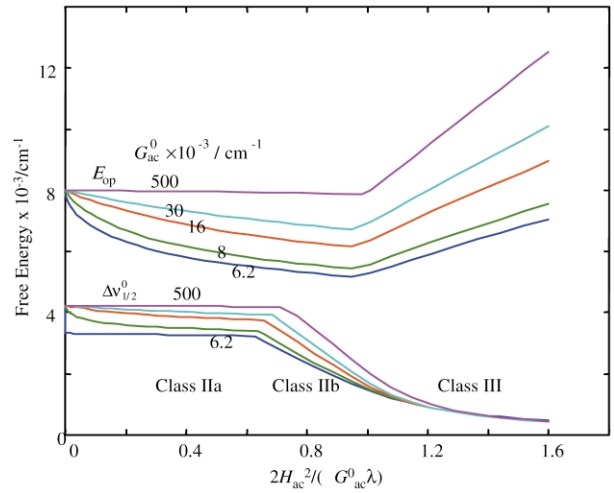

Fig. 15 Predictions of the three-state treatment for MMCT. E_{op} (top set) and $\Delta\nu_{1/2}^0$ (bottom set) *vs.* $2H_{ac}^2/(\Delta G_{ac}^0\lambda)$ for different values of ΔG_{ac}^0 (λ_{ab} = 8000 cm^{-1} and λ_{ac} = 2000 cm^{-1}).

ΔG_{ac}^0 have similar effects on the energy surfaces and spectra. This behavior contrasts significantly with two-state behavior in which E_{op} remains equal to λ until the Class II–III transition. Moreover, for a given value of the effective electronic coupling the bands are narrower in the three-state than in the two-state treatment. In the Class III region, E_{op} increases with increasing

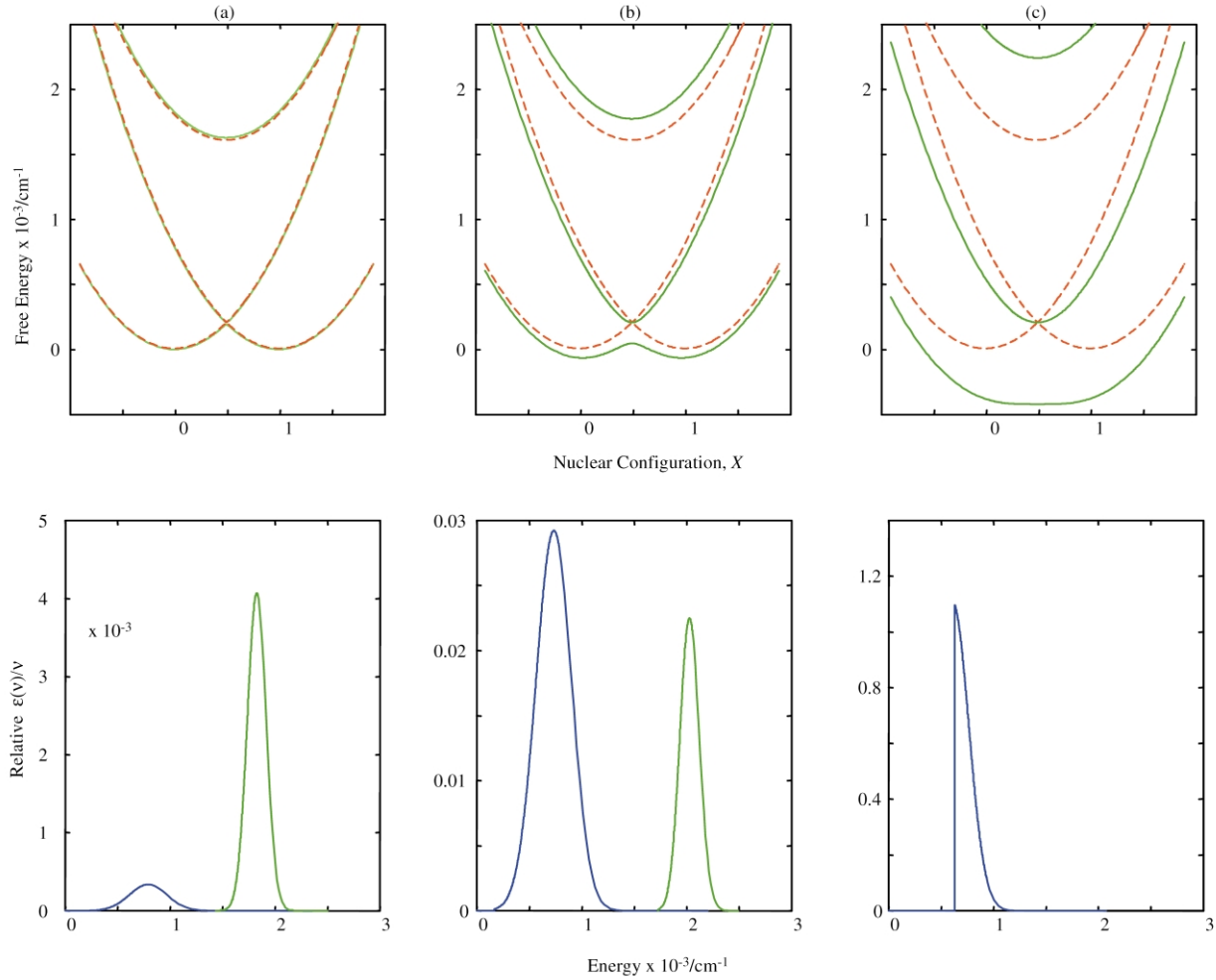

Fig. 14 Band Shape predictions from the three-state treatment. Plots of free energy *vs.* the nuclear configuration coordinate, X (top set) and relative $\varepsilon(\nu)/\nu$ *vs.* $h\nu$ (bottom set) for a symmetric mixed-valence system for increasing values of $2H_{ac}^2/(\Delta G_{ac}^0\lambda)$ with λ_{ab} = 8000 cm^1, λ_{ac} = 2000 cm^{-1} and ΔG_{ac}^0 = 16000 cm^{-1}. Both MMCT (lower energy) and MLCT/LMCT (high energy) bands are shown. The values of $2H_{ac}^2/(\Delta G_{ac}^0\lambda)$ (H_{ac}, cm^{-1} for (a), (b) and (c) are 0.02 (1130), 0.2 (1380) and 1.0 (8000), respectively. The values of $\varepsilon(\nu)/\nu$ are scaled to yield an oscillator strength proportional to the square of the calculated transition dipole moment, μ_{12}. The maximum values of $\varepsilon(\nu)/\nu$ for the low and high energy bands in (a), (b), (c) and (d) are 3.0×10^{-4}, 4.1×10^{-3}; 0.29, 0.23; and 1.1, 3.2×10^{-30}, respectively. See Fig. 3 for comparable two-state plots.

H_{ac}, but with a slope that diminishes as the mediating state drops in energy. Furthermore, the MLCT (LMCT) transition increases in energy with increasing H_{ac}, with the shifts being greater than for the MMCT transition (Fig. 14) because the magnitude of H_{ac} affects the lowest and highest adiabatic surfaces in opposite directions. Note that while the Class II–III transition occurs at $2H_{eff} = \lambda$ in the 'equivalent' two-state (superexchange) treatment it occurs somewhat earlier in the three-state treatment.

As found for the two-state model (Fig. 3), the MMCT band is truncated on the low-energy side as the system moves from Class II to Class III by virtue of increased coupling, increasing H_{ab} in the two-state case and increasing $H_{ac} = H_{bc}$ in the three-state case. Truncation of the MLCT/LMCT band also occurs as the lowest and highest adiabatic three-state surfaces become increasingly nested.

Fig. 16 and 17 present the dependences of Γ [eqn. (34)] and the transition moment on the three-state coupling parameter. The transition moment is calculated using (see ESI†)

$$\mu_{ij} = \frac{1}{2}(c^*_{bi}c_{bj} - c^*_{ai}c_{aj})(\mu_b - \mu_a) \qquad (39c)$$

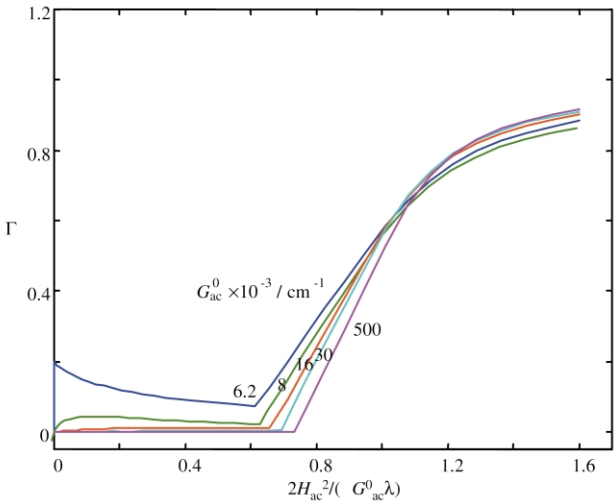

Fig. 16 Spectral predictions of the three-state treatment. Γ *vs.* $H_{ac}^2/(\Delta G^0_{ac}\lambda)$ for ΔG^0_{ac} = 6200 (top curve), 8000, 16000, 32000, and 500000 cm^{-1} (λ = 8000 cm^1).

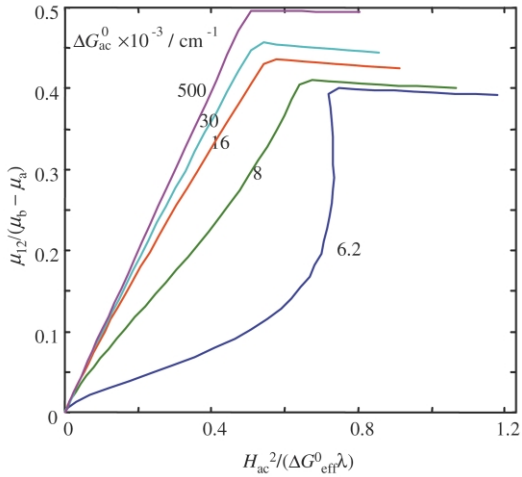

Fig. 17 Band intensity predictions (MMCT) of the three-state treatment. Plot of $\mu_{12}/(\mu_b - \mu_a)$ *vs.* $H_{ac}^2/(\Delta G_{eff}\lambda)$ for ΔG^0_{ac} = 6200 (bottom curve), 8000, 16000, 32000, and 500000 cm^{-1} (λ_{ab} = 8000 and λ_{ac} = 2000 cm^{-1}). When the third state lies sufficiently high (top curve), the slope given by the equivalent two-state model is observed.

In the equivalent two-state model for MMCT transitions the value of $\mu_{12}/(\mu_b - \mu_a) = H_{eff}/\lambda$ where H_{eff} is given by eqn. (39a). The figure shows that for very large ΔG^0_{ac} the equivalent two-state model is a good approximation of the three-state model. As ΔG^0_{ac} decreases the slope becomes less than 1; however, an essentially linear relationship between $\mu_{12}/(\mu_b - \mu_a)$ and H_{eff}/λ is maintained until $\Delta G^0_{ac} \approx \lambda$. This is seen in Fig. 17 for the curve with ΔG^0_{ac} = 8000 cm^{-1}. When $\Delta G^0_{ac} < \lambda$ the equivalent two-state model is no longer valid. In the Class III region the two-state model predicts $\mu_{12}/(\mu_b - \mu_a)$ = 1/2 while the three-state model has a limiting value that is dependent on ΔG^0_{ac} and λ. However the equivalent-two-state model gives transition moments that are within 80% of those given by the three-state model when $\Delta G^0_{ac} > \lambda$.

Note that the B $\rightarrow$ A 'MLCT/LMCT' transition in the Class III system has no intensity in this three-state treatment because the dipole moments of the initial and final diabatic states are both equal to $(\mu_a + \mu_b)/2$. Nevertheless the bridge MLCT/LMCT states couple to the ground diabatic states because $H_{ac} = H_{bc} \neq 0$.

The symmetrical vibration mode

An additional important feature of a more comprehensive three-state model is the inclusion of the symmetric vibrational mode[36] The resulting energy surfaces are illustrated in Fig. 18. This

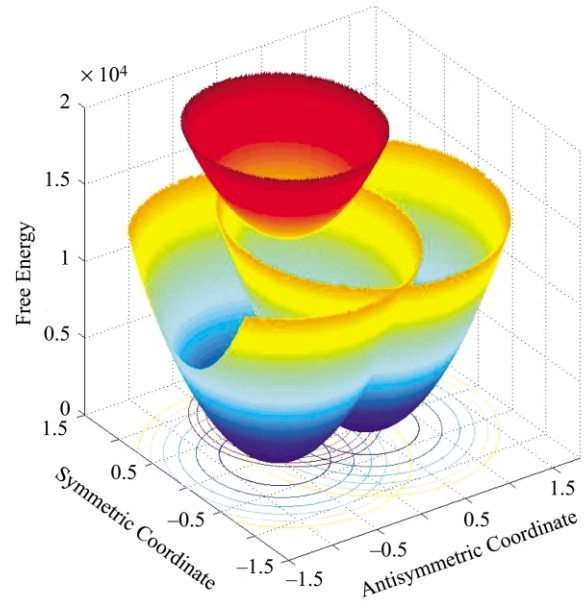

Fig. 18 Three-dimensional diabatic energy surfaces for the initial, final and mediating (reduced or oxidized bridge) states illustrating the effect of including the symmetric vibrational mode. ΔG^0_{ac} = 12000; the minima in the antisymmetric and symmetric modes are at [−0.5, 0], [0.5, 0] and [0, 0.5] for the reactant, product and mediating diabatic states, respectively.

mode is normally omitted in the two-state treatment[37] because it simply translates the two energy surfaces.

The addition of the symmetric vibrational mode to the three-state model has only a modest effect on E_{op} and $\Delta\nu_{1/2}$ in the Class II region (compare Fig. 19 to Fig. 15). The point at which the full width starts to decrease due to the low energy cut-off is independent of ΔG^0_{ac}. In the Class III region the symmetric mode effectively broadens the absorption band. However, not as much width is gained on adding the symmetric vibrational mode as was lost on going from the two-state to the three-state model. The effect on Γ of including a third state is shown in Fig. 20. In the Class II region Γ is smaller, while in the Class III region Γ becomes a function of ΔG^0_{ac} as the coupling increases.

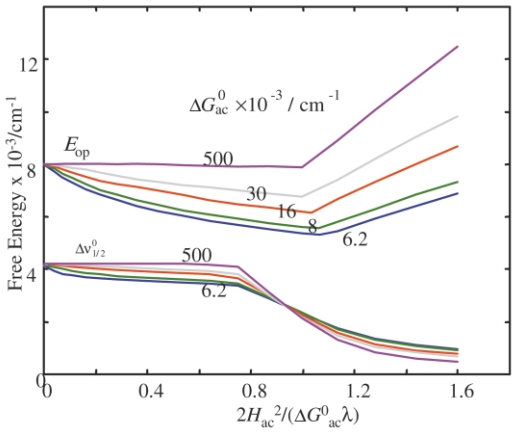

Fig. 19 The consequences of including the symmetric vibrational mode in the three-state model on band energy and half width. E_{op} (top set) and $\Delta\nu^0_{1/2}$ (bottom set) *vs.* $H^2_{ac}/(\Delta G^0_{ac}\lambda)$ for ΔG^0_{ac} = 6200 (bottom curve), 8000, 16000, 30000, and 500000 cm^{-1} (λ_{ab} = 8000 cm^{-1}, with the minima in the antisymmetric and symmetric modes at [−0.5, 0], [0.5, 0] and [0, 0.5] for the reactant, product and mediating diabatic states, respectively. Compare Fig. 15).

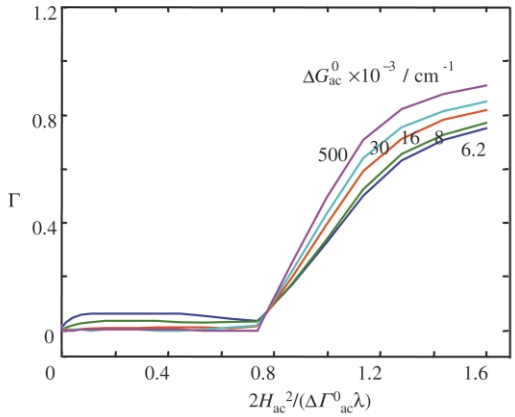

Fig. 20 The consequences of including the symmetric vibrational mode in the three-state model on Γ. Plot of Γ *vs.* $2H^2_{ac}/(\Delta G^0_{ac}\lambda)$ for ΔG^0_{ac} = 6200 (top curve), 8000, 16000, 30000, and 500000 cm^{-1} (λ_{ab} = 8000 cm^{-1}, with the minima in the antisymmetric and symmetric modes at [−0.5, 0], [0.5, 0] and [0, 0.5] for the reactant, product and mediating diabatic states, respectively).

5 A four-state model for the charge transfer transition

The above treatment, while helpful for systems in which only the transferring electron needs to be considered, is not applicable to systems with several d electrons. Symmetric D_{2h} Ru(II)–B–Ru(III) complexes such as the pyrazine-bridged dimer $[(NH_3)_5Ru]_2pz^{5+}$ fall into the latter category. For these systems at least three electrons need to be considered. A simple molecular orbital treatment (Fig. 6) of the delocalized system (Class III) in which a d_{xz} orbital on each ruthenium (z is the molecular axis and the x axis is perpendicular to the pyrazine plane) and a pyrazine π* orbital is considered and metal–ligand interactions are neglected yields two metal-centered orbitals (one combination of symmetry g and the other of symmetry u) and a bridge orbital of u symmetry. Interaction of the two u orbitals yields a bonding (B) and antibonding (A) pair resulting in three molecular orbitals: one bonding metal–ligand (predominantly metal) orbital, one nonbonding (N) metal orbital, and an antibonding metal–ligand (predominantly ligand) orbital. (see Fig. 6) The state wave function for the three-electron system is a product of the occupied molecular orbitals. The electron configurations of the four lowest energy states are shown below.

State	Population B	Population N	Population A	Designation	Sym-metry
1	↑ ↓	↑		GS (reactant)	*g*
2	↑	↑ ↓		MMCT (product)	*u*
3	↑ ↓		↑	MLCT1	*u*
4	↑	↓	↑	MLCT2	*g*

Free-energy surfaces

A four-state model requires the energies and electronic couplings of the diabatic (Mulliken–Hush) states, as well as their dipole moments. The metal-based diabatic states have minima at X = 0 and 1, while the ligand-based states are assumed to have minima at $X = 0.5 \pm \delta$ ($\delta \geqslant 0$). All diabatic states are assigned the same force constant (the same value as used in the previous sections). This results in different reorganization energies for the various transitions. The diabatic state energies are then

$$G_a = \lambda(X)^2$$

$$G_b = \lambda(X - 1.0)^2$$

$$G_c = \lambda(X - 0.5 + \delta)^2 + \Delta G^0_{ac}$$

$$G_d = \lambda(X - 0.5 - \delta)^2 + \Delta G^0_{ac}$$

and their minima are at 0, 1.0, $(0.5 - \delta)$ and $(0.5 + \delta)$, respectively. The dipole moment differences between the upper and lower states are assumed to be $(\mu_c - \mu_a) = (0.5 - \delta)(\mu_b - \mu_a)$ and $(\mu_d - \mu_a) = (0.5 + \delta)(\mu_b - \mu_a)$. All transition moments for the diabatic states are zero as required for the generalized Mulliken–Hush diabatic formalism.[16]

We consider both nondisplaced and displaced upper states corresponding to δ = 0 (Case 4A) and δ = 0.3 (Case 4B), respectively. In Case 4A the two upper states are degenerate for all X with minima located at X = 0.5 while in Case 4B the two upper states are horizontally displaced with minima at X = 0.2 and 0.8, respectively. This is illustrated in Fig. 21.

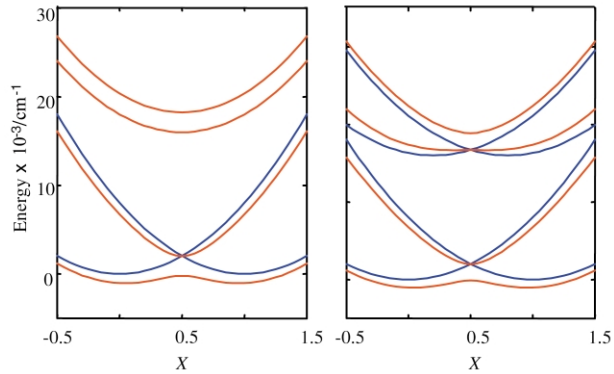

Fig. 21 Four-state free-energy surfaces for Case 4A (left) and Case 4B (right).

Mixing of the four diabatic states leads to four adiabatic states. As before, we assume no direct coupling between states a and b (H_{ab} = 0). We also assume there is no direct coupling between states c and d (H_{cd} = 0) and that the remaining couplings are equal ($H_{ac} = H_{ad} = H_{bc} = H_{bd}$). With weak coupling, states 1 and 2 are predominantly metal centered, while states 3 and 4 are mainly ligand centered. State 1 is stabilized and state 4 is destabilized and their separation increases with increasing coupling. While in Case 4A the energy of intermediate state 3 is equal to that of state c for all values of X, in Case 4B the energies of the two states are only equal at X = 0.5 (see Fig. 21).

At $X = 0.5$ the Hamiltonian can be solved analytically to yield the following energies for the adiabatic states

$$0, \Delta G_g, \frac{1}{2}\left(\Delta G_g \pm \left[\Delta G_g{}^2 + (4H_{ac})^2\right]^{1/2}\right)$$

where ΔG_g is the vertical difference between the energies of the diabatic metal-based states and the MLCT states at $X = 0.5$. For the case where $\Delta G_g >> H_{ac}$ we obtain the adiabatic energies:

$$0, \Delta G_g, -\frac{4H_{ac}^2}{\Delta G_g}, \Delta G_g + \frac{4H_{ac}^2}{\Delta G_g}$$

The effective two-state (superexchange) coupling can be defined as $2H_{ac}^2/\Delta G_g$, which is half the separation of the adiabatic metal-based states in the four-state model. This coupling is twice the superexchange coupling in the three-state model (eqn. (40a)) because there are now identical couplings to two MLCT states.

Absorption band energies, shapes, and intensities

The transition energies and transition moments can be calculated using the approach introduced earlier and by diagonalizing the Hamiltonian numerically. Not surprisingly, similar transition energies are calculated for the two cases at high couplings (Fig. 22). By contrast, because of different dipole moments of

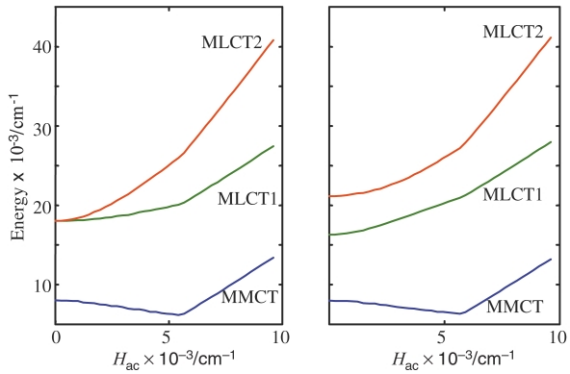

Fig. 22 MLCT and MMCT energies as a function of coupling energy for Case 4A (left) and Case 4B (right).

the MLCT states assumed for the two cases the calculated transition moments show both similarities and differences (Fig. 23).

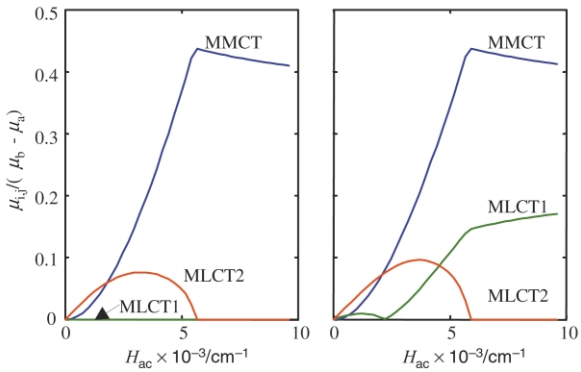

Fig. 23 Band intensities as a function of coupling energy for Case 4A (left) and Case 4B (right).

In both cases the transition moment for the high energy MLCT (1 to 4) transition becomes zero for Class III systems, as required by the symmetry. The transition moment for the low energy MLCT (1 to 3) transition remains equal to zero for Case 4A regardless of the electronic coupling. However, in Case 4B this transition is weak for weakly coupled Class II systems, but becomes the dominant MLCT transition for Class III systems. Case 4B corresponds more closely to what is observed, *i.e.*, Class III species retain "MLCT" bands. It is noteworthy that the MMCT band maximum and strength are insensitive to whether the upper states are nested or not. Furthermore, at high effective coupling, the MLCT energies are the same for Case A and B, because Case A has gone to the single minimum limit.

Other aspects of the spectra are similar to those found above for the two- and three-state models. The band shape becomes truncated on the low energy side and the band becomes narrower as the electronic coupling increases. The widths of the three bands are dependent on the values used for the force constants and the locations of the minima.

6 Conclusions

In a two-state description of an electron transfer process there is a minimum of two nuclear coordinates, one describing the solvent fluctuations and the other the intramolecular vibrational distortions of the reactants and products. The optical charge-transfer transition can occur at any of these solvent and vibrational (and rotational) configurations of the reactants, each weighted by the appropriate Boltzmann factor. The parameter $\Gamma = 1 - (\Delta\nu_{1/2})/(16\ln(2)RT)^{1/2}$ provides a useful criterion for determining whether a particular system is weakly coupled, moderately coupled, at the Class II–III transition, or strongly coupled. For a two-state model with $\lambda = 8000$ cm^{-1}, these four regimes correspond to $0 < \Gamma < 0.1$, $0.1 < \Gamma < 0.5$, $\Gamma \approx 0.5$ and $\Gamma > 0.5$, respectively, at room temperature. Similar considerations also apply to a three-state model in which the electron transfer is mediated by charge transfer to or from the bridging group. An additional feature of the three-state model is that a symmetrical vibration coordinate also needs to be included in addition to the antisymmetric vibrational coordinate normally considered in the two-state system. As discussed above, inclusion of the symmetric mode modifies the three-state energy surfaces and the shapes of the charge-transfer absorption bands. To reproduce qualitatively the fact that MLCT transitions are observed experimentally for strongly coupled systems, the four-state Case B is required.

7 Acknowledgements

This research was carried out at Brookhaven National Laboratory under contract DE-AC02-98CH10886 with the U.S. Department of Energy and supported by its Division of Chemical Sciences, Office of Basic Energy Sciences.

8 References

1 N. S. Hush, *Prog. Inorg. Chem.*, 1967, **8**, 391.
2 M. B. Robin and P. Day, *Adv. Inorg. Chem. Radiochem.*, 1967, **10**, 247.
3 K. D. Demadis, C. M. Hartshorn and T. J. Meyer, *Chem. Rev.*, 2001, **101**, 2655.
4 R. J. Crutchley, *Adv. Inorg. Chem.*, 1994, **41**, 273.
5 C. Creutz, *Prog. Inorg. Chem.*, 1983, **30**, 1.
6 C. Lambert and G. Nöll, *J. Am. Chem. Soc.*, 1999, **121**, 8434.
7 S. F. Nelsen, R. F. Ismagilov and D. A. Trieber, *Science*, 1997, **278**, 846.
8 S. F. Nelsen, *Chem. Eur. J.*, 2000, **6**, 581.

9 C. E. B. Evans, M. L. Naklicki, A. R. Rezvani, C. A. White, V. V. Kondratiev and R. J. Crutchley, *J. Am. Chem. Soc*., 1998, **120**, 13096.
10 K. D. Demadis, E.-S. El-Samanody, G. M. Coia and T. J. Meyer, *J. Am. Chem. Soc*., 1999, **121**, 535.
11 K. D. Demadis, G. A. Neyhart, E. M. Kober, P. S. White and T. J. Meyer, *Inorg. Chem*., 1999, **38**, 5948.
12 R. A. Marcus and N. Sutin, *Biochim. Biophys. Acta*, 1985, **811**, 265.
13 N. Sutin, *Prog. Inorg. Chem*., 1983, **30**, 441.
14 S. F. Nelsen, R. F. Ismagilov, K. E. Gentile and D. R. Powell, *J. Am. Chem. Soc*., 1999, **121**, 7108.
15 S. F. Nelsen and M. D. Newton, *J. Phys. Chem. A*, 2000, **104**, 10023.
16 R. J. Cave and M. D. Newton, *Chem. Phys. Lett*., 1996, **249**, 15.
17 S. B. Piepho, E. R. Krausz and P. N. Schatz, *J. Am. Chem. Soc*., 1978, **100**, 2996.
18 B. S. Brunschwig and N. Sutin, in *Electron Transfer in Chemistry*, ed. V. Balzani, Wiley-VCH, New York, 2001, Volume 2, p. 583.
19 C. P. Kubiak, personal communication, 2001.
20 T. Ito, T. Hamaguchi, H. Nagino, T. Yamaguchi, H. Kido, I. S. Zavarine, T. Richmond, J. Washington and C. P. Kubiak, *J. Am. Chem. Soc*., 1999, **121**, 4625.
21 C. Creutz, M. D. Newton and N. Sutin, *J. Photochem. Photobiol. A: Chem*., 1994, **82**, 47.
22 P. W. Atkins and R. S. Friedman, *Molecular Quantum Mechanics*, 3rd edn., Oxford Univ. Press, 1997, p. 509.
23 M. L. Naklicki and R. J. Crutchley, *J. Am. Chem. Soc*., 1994, **116**, 6045.
24 M. C. DeRosa, C. A. White, C. E. B. Evans and R. J. Crutchley, *J. Am. Chem. Soc*., 2001, **123**, 1396.
25 B. S. Brunschwig and N. Sutin, *Coord. Chem. Rev*., 1999, **187**, 233.
26 R. J. Crutchley and M. L. Naklicki, *Inorg. Chem*., 1989, **28**, 1955.
27 C. Creutz and M. H. Chou, *Inorg. Chem*., 1987, **26**, 2995.
28 S. P. Best, R. J. H. Clark, R. C. S. McQueen and S. Joss, *J. Am. Chem. Soc*., 1989, **111**, 548.
29 L. M. Baraldo, P. Forlano, A. R. Parise, L. D. Slep and J. A. Olabe, *Coord. Chem. Rev*., 2001, **219–221**, 881.
30 L. D. Slep, S. Pollak and J. A. Olabe, *Inorg. Chem*., 1999, **38**, 4369.
31 J. T. Hupp and T. J. Meyer, *Inorg. Chem*., 1987, **26**, 2332.
32 P. Chen and T. J. Meyer, *Chem. Rev*., 1998, **98**, 1439.
33 K. W. Lau, A. M.-H. Hu, M. H.-J. Yen, E. F. Fung, S. Grzybicki, R. Matamoros and J. C. Curtis, *Inorg. Chim. Acta*, 1994, 226.
34 S. Larsson, *J. Am. Chem. Soc*., 1981, **103**, 4034.
35 S. Larsson, *J. Phys. Chem*., 1984, **88**, 1321.
36 J. R. Reimers and N. S. Hush, *Chem. Phys*., 1996, **208**, 177.
37 M. J. Ondrechen, J. Ko and L. L. Root, *J. Phys. Chem*., 1984, **88**, 5919.